AD-A084 256 ARIZONA UNIV TUCSON ENGINEERING EXPERIMENT STATION F/G 20/14
EXTERIOR-INTERIOR APERTURE COUPLING OF A RECTANGULAR CAVITY WIT--ETC(U)
MAR 80 W A JOHNSON AFOSR-77-3462

UNCLASSIFIED AFOSR -TR-80-0413 NL

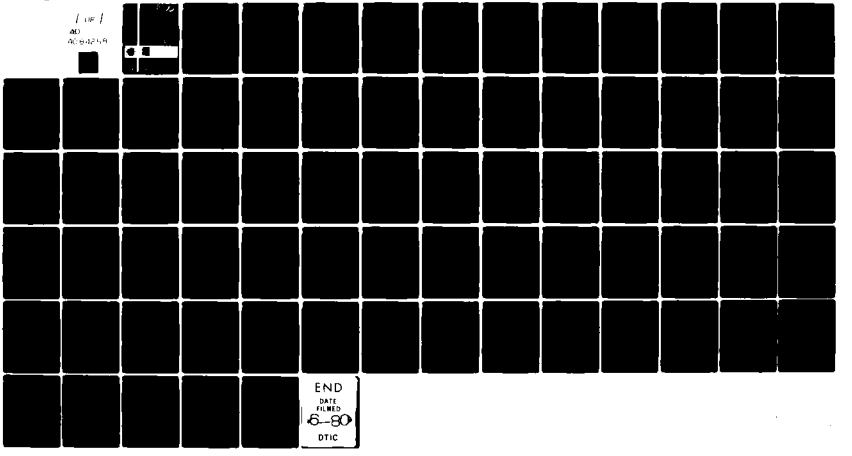

END
DATE FILMED
6-80
DTIC

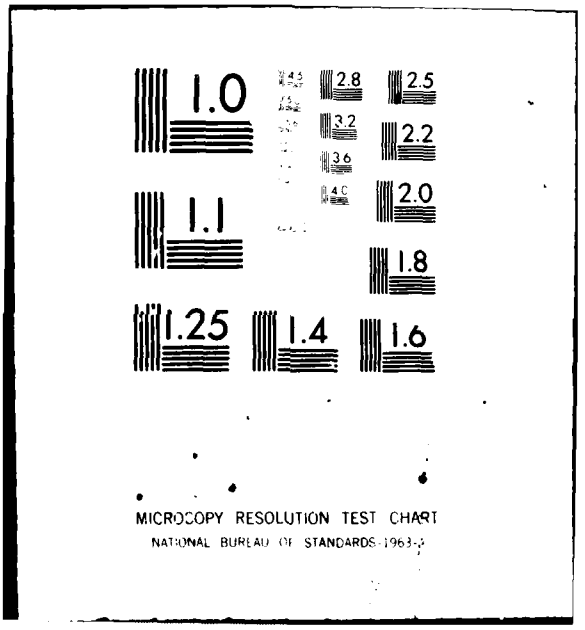
1.0
2.8
2.5
3.2
2.2
3.6
4.0
2.0
1.1
1.8
1.25
1.4
1.6
MICROCOPY RESOLUTION TEST CHART
NATIONAL BUREAU OF STANDARDS-1963-A

AFOSR-TR- 80-0419

LEVEL II

Final Technical Report

Grant No. AFOSR 77-3462

EXTERIOR-INTERIOR APERTURE COUPLING OF A RECTANGULAR CAVITY WITH WIRE OBSTACLE FINAL PHASE

for

Department of the Air Force
AIR FORCE OFFICE OF SCIENTIFIC RESEARCH
Bolling Air Force Base
Washington, D. C. 20332

by

William Arthur Johnson

31 March 1980

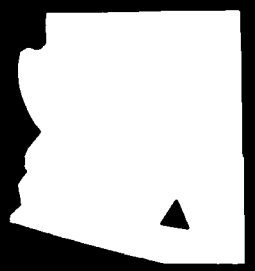

ENGINEERING EXPERIMENT STATION
COLLEGE OF ENGINEERING
THE UNIVERSITY OF ARIZONA
TUCSON, ARIZONA

Unclassified

SECURITY CLASSIFICATION OF THIS PAGE (When Data Entered)

REPORT DOCUMENTATION PAGE	READ INSTRUCTIONS BEFORE COMPLETING FORM
1. REPORT NUMBER: AFOSR-TR-80-0413	2. GOVT ACCESSION NO.: AD-A084 258
3. RECIPIENT'S CATALOG NUMBER	
4. TITLE (and Subtitle): EXTERIOR-INTERIOR APERTURE COUPLING OF A RECTANGULAR CAVITY WITH WIRE OBSTACLE	5. TYPE OF REPORT & PERIOD COVERED: Final Report 8/30/79 - 1/31/80
	6. PERFORMING ORG. REPORT NUMBER
7. AUTHOR(s): William Arthur/Johnson	8. CONTRACT OR GRANT NUMBER(s): AFOSR-77-3462
9. PERFORMING ORGANIZATION NAME AND ADDRESS: Engineering Experiment Station, University of Arizona, Tucson, Arizona 85721	10. PROGRAM ELEMENT, PROJECT, TASK AREA & WORK UNIT NUMBERS: 61102F 2301/A3
11. CONTROLLING OFFICE NAME AND ADDRESS: Air Force Office of Scientific Research/NP, Air Force Systems Command, USAF, Bolling Air Force Base, D. C. 20332	12. REPORT DATE: 31 March 1980
	13. NUMBER OF PAGES: Seventy (70)
14. MONITORING AGENCY NAME & ADDRESS (if different from Controlling Office)	15. SECURITY CLASS. (of this report): Unclassified
	15a. DECLASSIFICATION/DOWNGRADING SCHEDULE

16. DISTRIBUTION STATEMENT (of this Report)

Approved for public release; distribution unlimited.

17. DISTRIBUTION STATEMENT (of the abstract entered in Block 20, if different from Report)

18. SUPPLEMENTARY NOTES

19. KEY WORDS (Continue on reverse side if necessary and identify by block number)

Rectangular Cavity
Dyadic Green's Function
Shielding
Singular Integral Equations

20. ABSTRACT (Continue on reverse side if necessary and identify by block number)

In this work, the exterior-interior coupling problem of a cavity backed aperture in a perfectly conducting infinite sheet is considered. The cavity is assumed to be rectangular and contains a perfectly conducting obstacle. For numerical considerations the obstacle is taken to be a straight, thin wire, oriented perpendicular to one of the cavity walls. The problem is formulated in the frequency domain with an $e^{i\omega t}$ time dependence.

DD FORM 1473 EDITION OF 1 NOV 65 IS OBSOLETE

Unclassified

20. (cont'd.)

The dyadic formulation of this vector electromagnetic boundary value problem is given. The controversy over the longitudinal wave functions and their contribution to field dyads is resolved. Specific attention is given to the singularities and completeness of the Green's dyads' eigenfunction expansions.

Numerically tractable integral equations for the aperture electric fields and the wire currents are obtained. A summation method is developed for evaluation of otherwise slowly converging eigenfunction expansions of potentials dyads when source and observation points become close.

The numerical reduction of the integral equations by the method of moments is described. The numerical results for the aperture fields and the wire currents disclose a minus sign discrepancy between the results and previous results of Seidel. A discussion is given which supports the sign in the present work.

Final Technical Report

EXTERIOR-INTERIOR APERTURE COUPLING OF A RECTANGULAR CAVITY WITH WIRE OBSTACLE FINAL PHASE

for

Department of the Air Force
AIR FORCE OFFICE OF SCIENTIFIC RESEARCH
Bolling Air Force Base
Washington, D. C. 20332

Grant No. AFOSR 77-3462

31 March 1980

Prepared by: William A. Johnson

William Arthur Johnson
Assistant Professor

Approved by:

D. G. Dudley
Professor

Department of Electrical Engineering
THE UNIVERSITY OF ARIZONA
Tucson, Arizona 85721

TABLE OF CONTENTS

LIST OF FIGURES

LIST OF FIGURES CONTINUED

LIST OF TABLES

CHAPTER 1

INTRODUCTION AND SUMMARY

This final report on AFOSR Grant No. 77-3462 is a technical description of exterior-interior aperture coupling of a plane electromagnetic wave to a rectangular cavity containing a wire obstacle. Portions of the research have been described in previous annual and interim reports. In addition, portions have been presented at meetings of the International Scientific Radio Union (URSI) and in a paper published in Radio Science (Johnson, Howard, and Dudley, 1979). All of the important analysis and results for the entire program are contained in this final report. In addition, we contemplate one additional journal article based on the final results contained herein.

The problem of coupling electromagnetic energy into a cavity through an aperture and excitation of current on a wire in the interior is one requiring considerable care both in formulation and numerical reduction. Essentially the procedure we have used is to begin with Maxwell's equations, produce vector Helmholtz equations for the electric and magnetic fields, and invert the ensuing second order vector differential operators through application of a dyadic Green's theorem. The results are expressions for the electric and magnetic fields that can be specialized as integral equations by taking the observation

points to the aperture and to the surface of the interior wire. The coupled integral equations produced are next solved by the method of moments, a procedure which transforms the integral equations into a matrix equation that can be numerically inverted.

To simplify the technical bookkeeping, we have formulated the problem in dyadic notation. This approach is particularly useful in displaying the various components in the Green's functions. One of the significant contributions of this study has been in the careful construction of the dyads and their evaluation in regions where they become singular. This subject is treated in detail in our journal article recently published in Radio Science, referred to above. We have been particularly careful concerning the distributional character of some of the singularities and the completeness of the Green's dyadic eigenfunction expansions, a fact that has led to some controversy in the literature. We feel that our contributions have resolved some confusing statements on the longitudinal wave functions and we are confident of our results.

The numerical reduction has occupied a major portion of our time during the last year of the research. We have developed a summation method for evaluation of otherwise slowly converging eignefunction series and thereby have been able to significantly reduce the numerical processing time. We have discovered a sign discrepancy between our work and that of Seidel (1978). Our analysis supports the sign obtained in our results.

In Chapter 2, we discuss the problem geometry and produce the formulation in the frequency domain. In Chapter 3, we discuss the scheme for numerical solution with particular attention to subdividing the matrix to be inverted by the method of moments. In Chapter 4, we discuss the special techniques developed to sum the series appearing in the various elements of the matrix. In Chapter 5, we give sample numerical results for aperture fields and wire currents. We have included an appendix describing our analysis of the sign difference between this work and that of Seidel.

As a footnote, we should like to point out a dissapointment in one phase of the work. We had hoped to be able to provide some transient results for the wire current by obtaining the currents at various positions along the wire over a wide range of frequencies, multiplying by the spectrum of a suitable input pulse, and taking the numerical inverse Fourier transform. Indeed, Figures 21 and 22 are representative of our efforts in this regard. Unfortunately the resonances are so narrow (in engineering terms, the Q is extremely high) that we could not obtain a causal inverse transform. In other words, the resonance is so localized, it is as if we were attempting to take the inverse transform of a delta function. We verified our difficulties by creating an RLC circuit model, solving for the current in the frequency domain, and attempting a numerical inverse transform. All goes well until one selects a value for the resistance small enough to again produce a very high Q situation. At this point all codes we have tried for performance of the numerical

inverse start failing. We believe that this problem can be solved by analytic continuation of the frequency variable ω away from the real axis to avoid the poles of the transfer function that are located close to the axis. Since attempting such a procedure requires a major set of changes in our computer program we have not tried to do this.

CHAPTER 2

FREQUENCY DOMAIN FORMULATION

The frequency domain version of the boundary value problem of Figure 1 is now considered by specializing the exterior source to that of a time harmonic $e^{i\omega t}$ plane wave. The problem formulation of this section will result in a numerically tractable system of coupled integro-differential equations for the thin wire currents and tangential aperture electric fields. Once these wire currents and tangential aperture electric fields are determined, fields anywhere in the exterior or interior regions may be computed by use of the appropriate Green's functions.

First potential dyads for cavity interior and exterior half-space are constructed. Next these dyads are used to obtain integral representations of the electromagnetic fields in each region. These integral representations are given in terms of the unknown tangential aperture electric fields and wire currents. Continuity of the aperture's tangential electric fields and the boundary condition that the tangential component of the electric field is zero along the wire are enforced to yield a system of coupled integro-differential equations for the unknown aperture electric fields and wire currents.

The potential Green's dyads for the exterior half-space and cavity interior are now constructed. The frequency domain solution of Maxwell's equations driven by electric currents may by expressed as

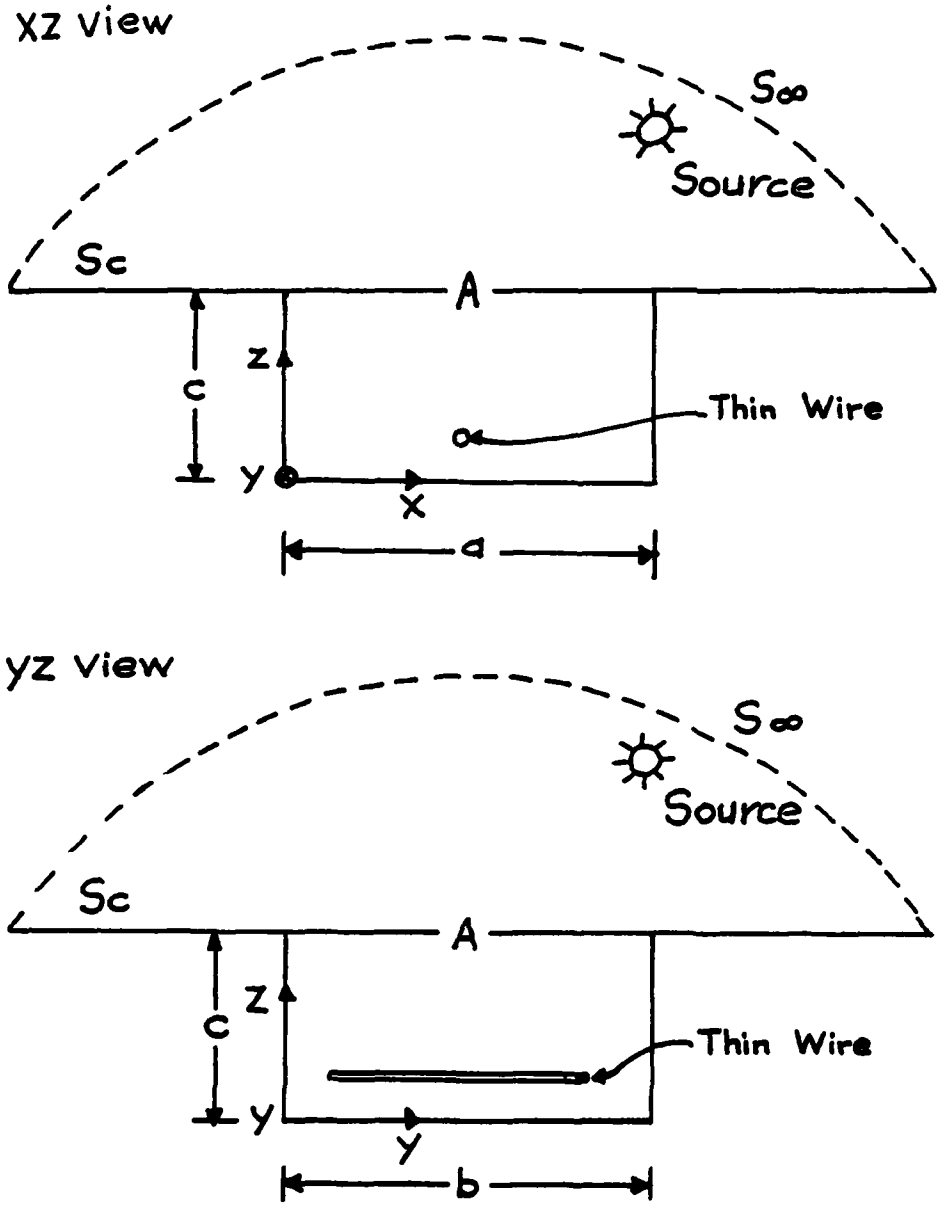

Figure 1. Problem Geometry.

$$\bar{E} = \frac{1}{i\omega\varepsilon\mu} (k^2 + \nabla\nabla\cdot)\bar{A} \tag{2.1a}$$

$$\bar{H} = \frac{\nabla x \bar{A}}{\mu} \tag{2.1b}$$

where

$$\left.\begin{aligned} -(\nabla^2 + k^2)\bar{A} &= \mu\bar{J} \\ \bar{n} \times \bar{A} &= 0 \\ \nabla \cdot \bar{A} &= 0 \end{aligned}\right\} \quad \text{on a perfect electric conductor (p.e.c.).} \tag{2.1c}$$

In (2.c) $\bar{n}$ denotes a unit normal vector.
The radiation condition at infinity and Meixner's edge condition [Meixner 1972] are imposed where appropriate to insure a unique solution. Similarly the solution of Maxwell's equations driven by magnetic currents is given by

$$\bar{H} = \frac{1}{i\omega\varepsilon\mu} (k^2 + \nabla\nabla\cdot)\bar{F} \tag{2.2a}$$

$$\bar{E} = -\frac{\nabla x \bar{F}}{\varepsilon} \tag{2.2b}$$

where

$$\left.\begin{aligned} -(\nabla^2 + k^2)\bar{F} &= \varepsilon\bar{M} \\ \bar{n} \times (\nabla x \bar{F}) &= 0 \\ \bar{n} \cdot \bar{F} &= 0 \end{aligned}\right\} \quad \text{on a p.e.c.} \tag{2.2c}$$

Solutions of the above systems (2.1) and (2.2) may be obtained by use of the corresponding magnetic and electric vector potential dyads $\bar{\bar{G}}_A$ and $\bar{\bar{g}}_F$. The magnetic potential dyad satisfies

$$-(\nabla^2 + k^2)\ \bar{\bar{G}}_A(\bar{r}|\bar{r}') = \bar{\bar{I}}\ \delta(\bar{r}-\bar{r}') \tag{2.3}$$

$$\left.\begin{aligned} \bar{n} \times \bar{\bar{G}}_A(\bar{r}|\bar{r}') &= 0 \\ \nabla \cdot \bar{\bar{G}}_A(\bar{r}|\bar{r}') &= 0 \end{aligned}\right\} \quad \text{on a p.e.c.}$$

where $\bar{\bar{I}}$ is the identy dyad. Similarly the electric vector potential dyad satisfies

$$-(\nabla^2 + k^2)\bar{\bar{g}}_F(\bar{r}|\bar{r}') = \bar{\bar{I}}\,\delta(\bar{r}-\bar{r}') \tag{2.4}$$

$$\left.\begin{aligned} \bar{n} \times (\nabla \times \bar{\bar{g}}_F(\bar{r}|\bar{r}')) &= 0 \\ \bar{n} \cdot \bar{\bar{g}}_F(\bar{r}|\bar{r}') &= 0 \end{aligned}\right\} \text{ on a p.e.c.}$$

Since these potential dyads are diagonal the exterior half-space dyads, denoted by the superscript "hs", may be constructed by image theory. The results are presented in Table 1. Since systems (2-3) and (2-4) determine self-adjont boundary value problems, the interior cavity dyads, denoted by superscript "c", may be given in terms of their complete eigenfunction expansions. These expansions are given in Table 2. The corresponding field dyads may be obtained by differenation, however they are highly singular and should be interpreted as distributions (Johnson, Howard, and Dudley, 1979).

Table 1. Potential Dyads for The Exterior Half-space*

$$\bar{\bar{G}}_A^{hs}(\bar{r}|\bar{r}') = \begin{bmatrix} \psi(\bar{r}|\bar{r}') - \psi_i(\bar{r}|\bar{r}') & 0 & 0 \\ 0 & \psi(\bar{r}|\bar{r}') - \psi_i(\bar{r}|\bar{r}') & 0 \\ 0 & 0 & \psi(\bar{r}|\bar{r}') + \psi_i(\bar{r}|\bar{r}') \end{bmatrix}$$

$$\bar{\bar{G}}_F^{hs}(\bar{r}|\bar{r}') = \begin{bmatrix} \psi(\bar{r}|\bar{r}') + \psi_i(\bar{r}|\bar{r}') & 0 & 0 \\ 0 & \psi(\bar{r}|\bar{r}') + \psi_i(\bar{r}|\bar{r}') & 0 \\ 0 & 0 & \psi(\bar{r}|\bar{r}') - \psi_i(\bar{r}|\bar{r}') \end{bmatrix}$$

where

$$\psi(\bar{r}|\bar{r}') = \frac{e^{-ikR}}{4\pi R}$$

$$\psi_i(\bar{r}|\bar{r}') = \frac{e^{-ikR_i}}{4\pi R_i} .$$

$$R = [(x-x')^2 + (y-y')^2 + (z-z')^2]^{\frac{1}{2}}$$

and

$$R_i = [(x-x')^2 + (y-y')^2 + (z+z'-c)^2]^{\frac{1}{2}} .$$

*The problem geometry is given in Figure 1.

Table 2. Potential Dyadic Green's Functions for A Rectangular Cavity*

$$\bar{\bar{G}}_A^c(\bar{r}\,\bar{r}') = \frac{1}{abc}\sum_{\ell,m,n=0}^{\infty} \frac{\varepsilon_\ell\,\varepsilon_m\,\varepsilon_n}{K_{\ell mn}^2 - k^2} \begin{bmatrix} (cc)_x(ss)_y(ss)_z & 0 & 0 \\ 0 & (ss)_x(cc)_y(ss)_z & 0 \\ 0 & 0 & (ss)_x(ss)_y(cc)_z \end{bmatrix}$$

and

$$\bar{\bar{g}}_F^c(\bar{r}\,\bar{r}') = \frac{1}{abc}\sum_{\ell,m,n=0}^{\infty} \frac{\varepsilon_\ell\,\varepsilon_m\,\varepsilon_n}{K_{\ell mn}^2 - k^2} \begin{bmatrix} (ss)_x(cc)_y(cc)_z & 0 & 0 \\ 0 & (cc)_x(ss)_y(cc)_z & 0 \\ 0 & 0 & (cc)_x(cc)_y(ss)_z \end{bmatrix}$$

where $(cc)_x(ss)_y(ss)_z = \cos(k_x x)\cos(k_x x')\sin(k_y y)\sin(k_y y')\sin(k_z z)\sin(k_z z')$, etc.

$$k_x = \frac{m\pi}{a}\,,\quad k_y = \frac{n\pi}{b}\,,\quad k_z = \frac{\ell\pi}{c}\,,\quad K_{\ell mn}^2 = k_x^2 + k_y^2 + k_z^2 - k^2$$

and

$$\varepsilon_i = \begin{cases} 1, & \text{if } i = 0 \\ 2, & \text{if } i \neq 0 \end{cases}$$

* The cavity dimensions are a,b, and c in the $\hat{x}$, $\hat{y}$, and $\hat{z}$ directions respectively.

Now that the appropriate Green's dyads have been constructed, they will be used to obtain integral representations of the electromagnetic fields in each region. The equivalence principle [Harrington 1961, p. 106] is used to obtain an equivalent problem for the exterior half-space as illustrated in Figure 2. In the equivalent problem the aperture has been shorted and the magnetic surface current $\bar{M}_s$ has been placed on the surface where the aperture was previously located. The magnetic surface current is chosen to make the electric field jump to its origional value just above the aperture surface. The equivalent problem for the interior region is obtained similarly and is illustrated in Figure 3.

It is convenient to separate the electromagnetic field in the exterior half-space into two terms. The short circuit fields, denoted by the superscript "sc", are those fields that would exist if the aperture were not present. These fields may easily be found by geometric optics. The fields due to the presence of the aperture or equivalently scattered by the magnetic surface current may be computed by use of the electric potential dyad $\bar{\bar{g}}_F^{hs}$ of Table 1 and (2.2). In particular the magnetic field in the exterior half-space is given by

$$\bar{H}(\bar{r}) = \bar{H}^{sc}(\bar{r}) + \frac{1}{i\omega\mu}(k^2+\nabla\nabla\cdot)\iint_A \bar{\bar{g}}_F^{hs}(\bar{r}|\bar{r}')\ \bar{M}_s(\bar{r}')\ ds' \qquad (2.5)$$

where A is the aperture surface. The first term on the right of (2.5) is the short circuit magnetic field, the second is the

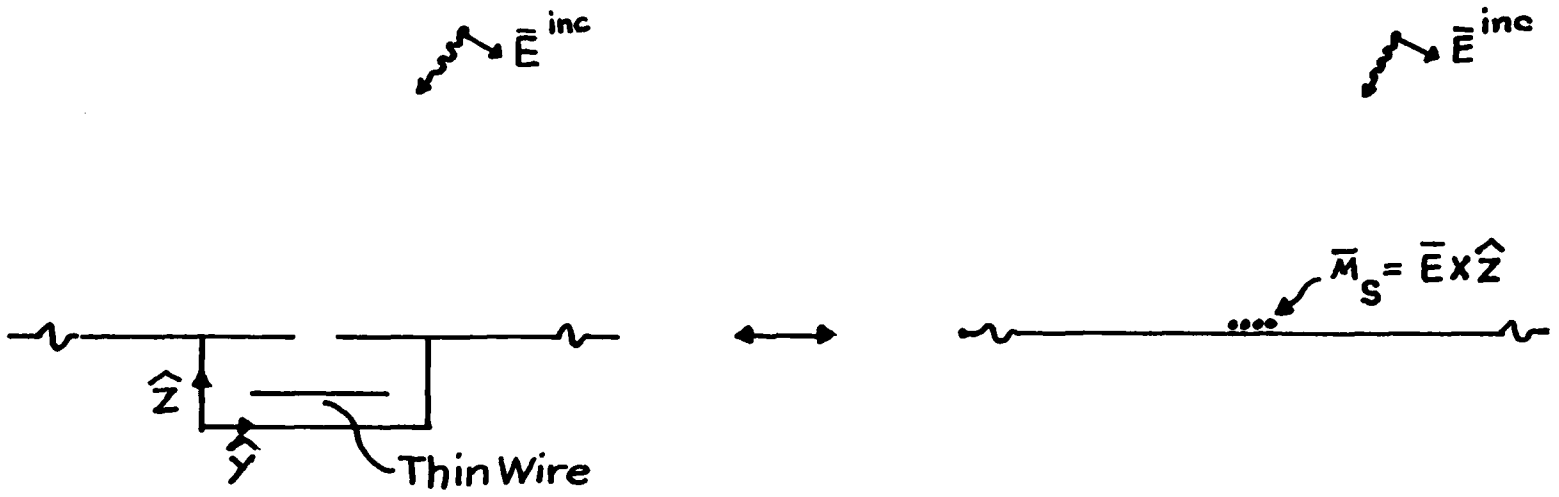

Figure 2. Equivalent Problem for The Exterior Region

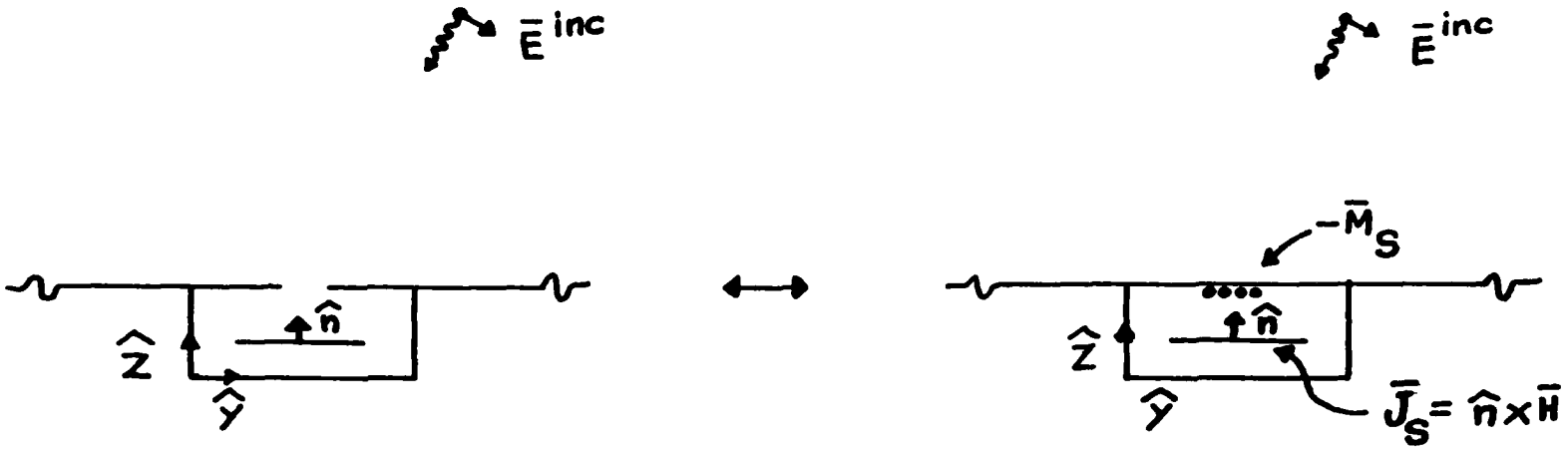

Figure 3. Equivalent Problem For The Interior Region.

magnetic field due to the presence of the aperture. The electric field for the exterior half-space may be found similarly by use of (2.2b) and (2.2c).

The fields in the cavity interior (Figure 3) are the sum of fields due to magnetic surface current plus the fields scattered by the wire. These fields may be obtained by use of the cavity potential dyads (Table 2) and (2.1) through (2.4). The magnetic field in the cavity interior is given by

$$\bar{H}(\bar{r}) = \frac{-1}{i\omega\mu}(k^2+\nabla\nabla\cdot)\iint_A \bar{\bar{g}}_F^c(\bar{r}|\bar{r}')\bar{M}_s(\bar{r}')ds' + \nabla \times \iint \bar{\bar{G}}_A^c(\bar{r}|\bar{r}')\bar{J}(\bar{r}')ds'. \quad (2.6)$$

The electric field in the cavity interior may be found in a similar manner.

Note that by construction the equivalent problems (Figures 2 and 3) satisfy continuity of the electric field across the aperture. Before enforcing continuity of the aperture's tangential magnetic field, it is recalled that under the thin wire assumptions of Section 1 all current is directed along the wire axis. Thus continuity of the apertures tangential magnetic field plus (2.5) and (2.6) yield

$$2i\omega\mu\, H_y^{inc}(\bar{r}) = (k^2+\frac{\partial^2}{\partial y^2})\iint_A [g_F^{hs,yy}(\bar{r}|\bar{r}') + g_F^{c,yy}(\bar{r}|\bar{r}')]E_x(\bar{r}')ds' \quad (2.7a)$$

$$-\frac{\partial^2}{\partial y\partial x}\iint_A [g_F^{hs,xx}(\bar{r}|\bar{r}') + g_F^{c,xx}(\bar{r}|\bar{r}')]E_y(\bar{r}')ds'$$

and

$$-2i\omega\mu\, H_x^{inc}(r) = (k^2 + \frac{\partial^2}{\partial x^2}) \iint_A [g_F^{hs,xx}(\bar{r}|\bar{r}') + g_F^{c,xx}(\bar{r}|\bar{r}')]\, E_y(\bar{r}')ds' \tag{2.7b}$$

$$\frac{-\partial^2}{\partial y \partial x} \iint_A [g_F^{hs,yy}(\bar{r}|\bar{r}') + g_F^{c,yy}(\bar{r}|\bar{r}')] E_x(\bar{r}')ds' + i\omega\mu \frac{\partial}{\partial z} \iint_W G_A^{c,yy}(\bar{r}|\bar{r}') J_y(\bar{r}')ds'.$$

The tangential component of the electric field along the wire is set to zero. This gives

$$0 = \frac{1}{i\omega\epsilon}(k^2 + \frac{\partial^2}{\partial y^2}) \iint_W G_A^{c,yy}(\bar{r}|\bar{r}') J_y(\bar{r}')ds' + \frac{\partial}{\partial z} \iint_A g_F^{c,xx}(\bar{r}|\bar{r}') E_y(\bar{r}')ds' \tag{2.7c}$$

Equation set (2.7) is a coupled system of integro-differential equations for the unknown aperture fields and wire currents. In the next section an efficient numerical solution scheme for this system will be presented.

CHAPTER 3

FREQUENCY DOMAIN SOLUTION SCHEME

A numerical solution scheme for the linear system of coupled integro-differential equations (2.7) derived in the previous section is now presented. The method of moments [Harrington 1968] with pulse expansions and point matching is used. As illustrated in Figures 4 and 5, the unknown, tangential, aperture electric field components are approximated by piecewise constant rectangular patches. The x component of the electric field is expressed as

$$E_x(\bar{r}') = \sum_{i=1}^{NE_x} e_{xi}\, P_{xi}(\bar{r}') \tag{3.8a}$$

where

$$P_{xi}(\bar{r}') = \begin{cases} 1 \text{ , if } \bar{r}' \text{ is in the } i^{th} \text{ rectangle of Fig. 4} \\ 0 \text{ , otherwise} \end{cases},$$

e_{xi} are unknown constant coefficients, and NE_x is the number of of nonzero E_x pulses. Similarly

$$E_y(\bar{r}') = \sum_{i=1}^{NE_y} e_{yi}\, P_{yi}(\bar{r}') \tag{3.8b}$$

where

$$P_{yi}(\bar{r}') = \begin{cases} 1, \text{ if } \bar{r}' \text{ is in the } i^{th} \text{ rectangle of Figure 5} \\ 0, \text{ otherwise} \end{cases},$$

e_{yi} are unknown coefficients, and NE_y is the number of nonzero E_y pulses.

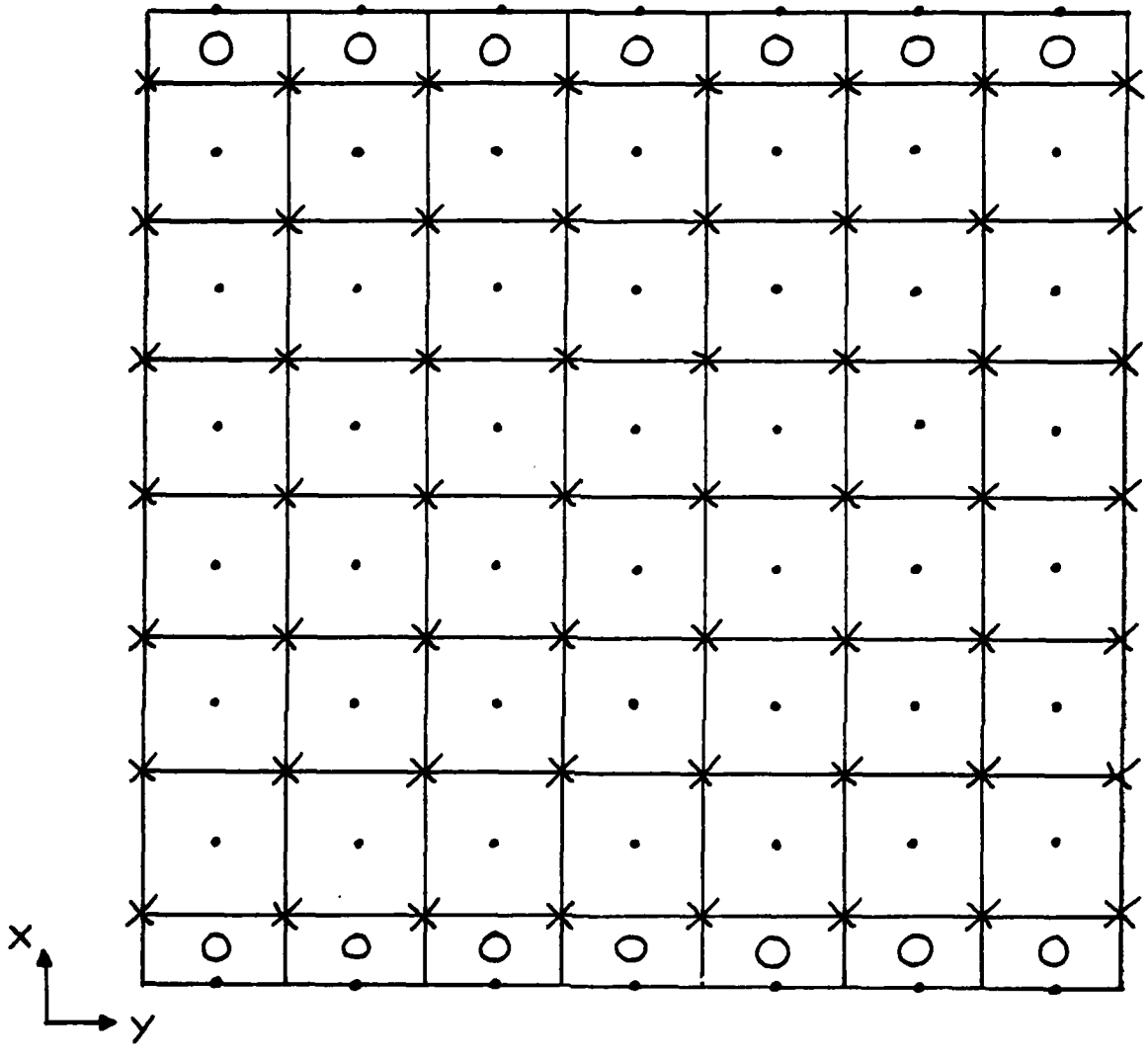

Figure 4. E_x Aperture Pulse Expansions and Finite Difference Grids for Potential Dyads.

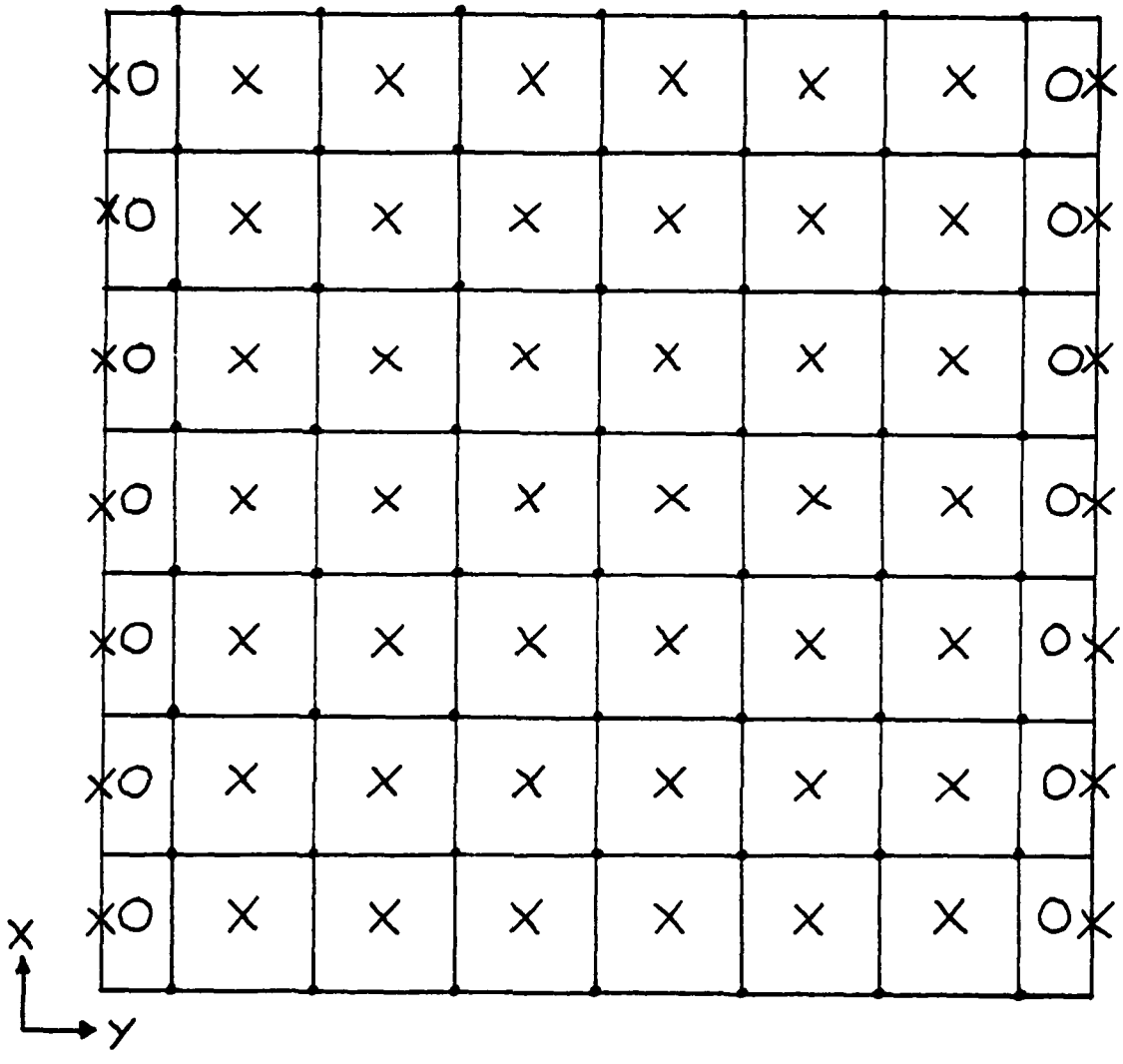

Finite Difference Grids : $\times\times$ g^{yy} grid

$\bullet\bullet$ g_F^{xx} grid

Figure 5. E_y Aperture Pulse Expansions and Finite Difference Grids for Potential Dyads.

Note that the E_x and E_y aperture pulse expansions (Figures 4 and 5) are offset. Centers of the E_x pulses correspond to corners of E_y pulses and vice versa. This will later allow efficient evaluation of the x and y derivatives in (2.7a) and (2.7b) by finite difference techniques. Wilton and Glission [1976] applied this technique, offsetting the expansion functions, to the problem of scattering from a rectangular plate.

Since J_y is assumed uniform about the wire circumference it is helpful to define the current I by

$$I(y') = 2\pi\, r_w\, J_y(y') \tag{3.9}$$

where r_w is the wire radius. Under the thin wire approximation all current is assumed to run along the wire's center [Seidel 1977, 1978]. This current is now approximated by (Figure 6)

$$I(y') = \sum_{i=1}^{NW} I_i\, P_{wi}(y') \tag{3.10}$$

where

$$P_{wi}(y') = \begin{cases} 1, & \text{if } y' \text{ belongs to the } i^{th} \text{ interval} \\ 0, & \text{otherwise} \end{cases},$$

I_i are the unknown current coefficients, and NW is the number of nonzero wire current pulses.

Enforcement of (3.7a) at the nonzero E_x aperture pulse centers, (3.7b) at the nonzero E_y aperture pulse centers, and (3.7c) at the wire surface points $(x_c + r_w, y_m, z_c)$, where x_c and z_c are the respective x and z corrdinates of the wire center and

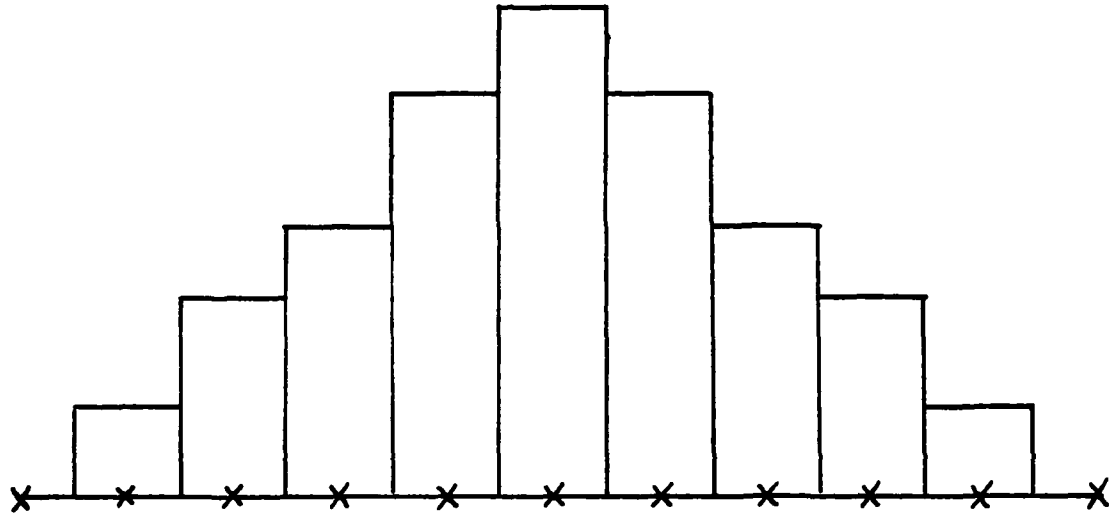

Figure 6. Wire Current Expansions and Finite Difference Grid.

y_m(m = 1, NW) are the nonzero wire current pulse center points, yields the $NE_x + NE_y + NW$ square matrix equation

$$\begin{bmatrix} T^{11}_{mi} & T^{12}_{mi} & 0 \\ T^{21}_{mi} & T^{22}_{mi} & T^{23}_{mi} \\ 0 & T^{32}_{mi} & T^{33}_{mi} \end{bmatrix} \begin{bmatrix} e_{xi} \\ e_{yi} \\ I_i \end{bmatrix} = \begin{bmatrix} f^1_m \\ f^2_m \\ 0 \end{bmatrix} . \tag{3.11}$$

The T submatrices are given by

$$T^{11}_{mi} = (k^2+\frac{\partial^2}{\partial y^2}) \iint_A [g_F^{hs,yy}(\bar{r}_m|\bar{r}') + g_F^{c,yy}(\bar{r}_m|\bar{r}')] P_{xi}(\bar{r}')dx'dy' \quad (m=1,NE_x;\ i=1,\ NE_x) \tag{3.12a}$$

$$T^{12}_{mi} = \frac{\partial^2}{\partial x \partial y} \iint_A [g_F^{hs,xx}(\bar{r}_m|\bar{r}') + g_F^{c,xx}(\bar{r}_m|\bar{r}')] P_{yi}(\bar{r}')dx'dy' \quad (m=1,\ NE_x;\ i=1,\ NE_y) \tag{3.12b}$$

$$T^{21}_{mi} = \frac{-\partial^2}{\partial x \partial y} \iint_A [g_F^{hs,yy}(\bar{r}_m|\bar{r}') + g_F^{c,yy}(\bar{r}_m|\bar{r}')] P_{xi}(\bar{r}')dx'dy' \quad (m=1,\ NE_y;\ i=1,NE_x) \tag{3.12c}$$

$$T^{22}_{mi} = (k^2+\frac{\partial^2}{\partial x^2}) \iint_A [g_F^{hs,xx}(\bar{r}_m|\bar{r}') + g_F^{c,xx}(\bar{r}_m|\bar{r}')P_{yi}(\bar{r}')dx'ds' \quad (m=1,\ NE_y;i=1,NE_y) \tag{3.12d}$$

$$T^{23}_{mi} = \frac{i\omega\mu}{2\pi} \frac{\partial}{\partial z} \iint_W G_A^{c,yy}(\bar{r}_m|\bar{r}')P_{wi}(y')dy'd\phi' \quad (m=1,NE_y;i=1,NW) \tag{3.12e}$$

$$T_{mi}^{32} = \frac{\partial}{\partial z} \iint_A g_F^{c,xx}(\bar{r}_m|\bar{r}')\ P_{yi}(\bar{r}')dx'dy' \quad (m=1,NW;i=1,NE_y) \tag{3.12f}$$

$$T_{mi}^{33} = \frac{1}{i\omega\varepsilon 2\pi}(k^2 + \frac{\partial^2}{\partial y^2}) \iint_W G^{c,yy}(\bar{r}_m|\bar{r}')P_{wi}(y')dy'd\phi' \quad (m=1,NW;i=1,NW) \tag{3.12g}$$

The forcing function's components are

$$f_m^1 = 2i\omega\mu\ H_y^{inc}(\bar{r}_m) \quad (m=1,NE_x) \tag{3.13a}$$

and

$$f_m^2 = -2i\omega\mu\ H_x^{inc}(\bar{r}_m) \quad (m=1,NE_y). \tag{3.13b}$$

Once the T matrix elements are obtained the unknown aperture field and wire current coefficients may be calculated by Gaussian elimination.

Evaluation of the T matrix elements (3.12a - 3.12d) is now considered. To avoid kernels that become highly singluar as $\bar{r}_m$ approaches $\bar{r}'$, the derivatives are kept outside the integral signs and are evaluated by finite differences. The appropriate finite difference grids are illustrated in Figures 4 and 5. Thus, the problem of evaluating (3.12a - 3.12d) reduces to that of computing the $\hat{x}\hat{x}$ and $\hat{y}\hat{y}$ components of the electric vector potential dyads integrated over the aperture pulses (' coordinates) and matched at the appropriate pulse centers. The major obstacle to these computations is that the cavity dyads (Table 2) converge more and more slowly as the distance between $\bar{r}_m$ and $\bar{r}'$ becomes small. Summation techniques for these dyads are presented in the

next section. The half-space potential terms are evaluated by analytical integration of the singular terms, then Gaussian quadrature [Abramowitz and Stegun 1964, P. 887] is used to integrate the remaining terms.

Since the source and observation points in (3.12e) and (3.12f) remain distant the z derivatives may be brought under the integral signs. The remaining kernels consist of exponentially convergent infinite series which may be integrated term by term.

The derivatives on the wire potential terms (3.12g) are kept outside the integral and evaluated by finite differences (Figure 6). The major obstacle to evaluation of this term is the summation of a cavity potential dyad as the distance between source and observation points becomes small. Techniques for carrying out this summation are presented in the next section.

CHAPTER 4

EVALUATION OF CAVITY POTENTIAL TERMS

The final obstacle to the solution of our frequency domain problem is the matrix fill of elements involving the cavity vector potentials $\overline{\overline{g}}_F^c$, and $\overline{\overline{G}}_A^c$. In Table 2 these dyads are given in terms of their threefold infinite eigenfunction expansions. For source and observation points distant it will be seen that these expansions reduce to rapidly exponentially convergent double series. However, as source and observation points become close, these series become slowly convergent. This chapter develops an efficient means of evaluating the potential dyad $\overline{\overline{g}}_F^c(\bar{r}|\bar{r}')$ for aperture source and observation points close, under the restriction that ka (Figure 1) is less than π. The same technique will be used to evaluate $\overline{\overline{G}}_A^c(\bar{r}'|\bar{r})$ in (3.12g) under the thin-wire restriction.

Consideration is now given to the $\hat{x}\hat{x}$ component of the dyad $g_F^{c,xx}$. Similar techniques hold for $g^{c,yy}$. From Table 2 with z = z' = c (Figure 1)

$$g_F^{c,xx}(\bar{r}|\bar{r}') = \frac{1}{abc} \sum_{\substack{\ell=0 \\ m=1 \\ n=0}}^{\infty} \frac{\varepsilon_\ell \varepsilon_m \varepsilon_n}{K_{\ell mn}^2 - k^2} \sin(k_x x)\sin(k_x x')\cos(k_y y)\cos(k_y y') \tag{4.1a}$$

$$= S(|x-x'|,|y-y'|) + S(|x-x'|, y+y') - S(x+x', y+y')$$

$$- S(x+x', |y-y'|) \tag{4.1b}$$

where

$$S(X,Y) = \frac{1}{4abc} \sum_{\substack{\ell=0 \\ m=1 \\ n=0}}^{\infty} \frac{\varepsilon_\ell \varepsilon_m \varepsilon_n}{K_{\ell mn}^2 - k^2} \cos(k_x X) \cos(k_y Y) \ . \qquad (4.1c)$$

Since the terms of (4.1b) depend only on sums and differences of the respective source and observation points' components, the number of calculations in evaluating (3.12b) and (3.12d) is less than if (4.1a) were applied directly.

For source and observation points distant the threefold infinite series of (4.1c) may be reduced to a double sum that yields itself to rapid evaluation by digital computer. Equation (4.1c) is closed in Y [Gradshteyn and Ryzhik 1965] which yields

$$S(X,Y) = \frac{1}{2ac} \sum_{\substack{\ell=0 \\ m=1}}^{\infty} \frac{\varepsilon_\ell \cosh[\sqrt{k_x^2 + k_y^2 - k^2}\ (b-Y)]}{\sqrt{k_x^2 + k_y^2 - k^2}\ \sinh[\sqrt{k_x^2 + k_y^2 - k^2}\ b]} \cos(k_x X) \qquad (4.2a)$$

with ka (Figure 1) less than π. The series in (4.2a) is exponentially converging and readily evaluated provided that Y is not too small with respect to the aperture dimensions and not too close to 2b. Likewise if (4.1c) is closed in X one obtains

$$S(X,Y) = \frac{1}{4bc} \sum_{\substack{\ell=0 \\ n=0}}^{\infty} \varepsilon_\ell \varepsilon_n \ T(X) \cos(k_y Y) - \frac{1}{4abc} \sum_{\substack{\ell=0 \\ n=0}}^{\infty} \frac{\varepsilon_\ell \varepsilon_n \cos(k_y Y)}{k_y^2 + k_z^2 - k^2} \qquad (4.2b)$$

where

$$T(X) = \begin{cases} \dfrac{\cosh\left[\sqrt{k_y^2 + k_z^2 - k^2}\,(a-X)\right]}{\sqrt{k_y^2 + k_z^2 - k^2}\,\sinh\left[\sqrt{k_y + k_z - k^2}\,a\right]}, & \text{if } k_y^2 + k_z^2 - k^2 > 0 \\ \dfrac{-\cos\left[\sqrt{k^2 - k_y^2 - k_z^2}\,(a-X)\right]}{\sqrt{k^2 - k_y^2 - k_z^2}\,\sin\left(\sqrt{k^2 - k_y^2 - k_z^2}\,a\right)}, & \text{if } k_y^2 + k_z^2 - k^2 < 0 \end{cases}$$

Similar techniques may be used to close the second term of (4.2b). The result is a single finite series with know asympotic form [Abramowitz and Stegun 1970, p. 1005]. This this series may readily be evaluated. First termwise subtraction of the corresponding asymptotic term from the original series term yields a rapidly converging new series. Next the otherwise slowly converging asymptotic series is added to the modified series by its known analytical form. The first term of (4.2b) is exponentially convergent provided X is not too small or too close to 2a. In the aperture geometries considered (Figure 1), the only case where neither (4.2a) or (4.2b) yields itself readily to numerical evaluaticn is for both X and Y small compared to the cavity dimensions. Otherwise, Seidel [1977] has obtained an efficient method for numerical evaluation of these sums.

The remainder of this chapter is concerned with evaluation of (4.1c) near the source, that for $X = |x-x'|$ and $Y = |y-y'|$ small. Equation (4.1c) is closed in z, making use of Spiegel [1964, p. 189] and Gradshteyn and Ryzhik [1965, p. 40]. This yields

$$S(X,Y) = \frac{1}{2ab} \sum_{\substack{m=1 \\ n=o}}^{\infty} \varepsilon_n \, T(k_x^2 + k_y^2 - k^2) \cos(k_x X) \cos(k_y Y) \qquad (4.3)$$

where

$$T(k_x^2 + k_y^2 - k^2) = \begin{cases} \dfrac{\coth(c\sqrt{k_x^2 + k_y^2 - k^2}}{\sqrt{k_x^2 + k_y^2 - k^2}}, & \text{if } k_x^2 + k_y^2 - k^2 > 0 \\ \dfrac{-\cot(c\sqrt{k^2 - k_x^2 - k_y^2}}{\sqrt{k^2 - k_x^2 - k_y^2}}, & \text{if } k_x^2 + k_y^2 - k^2 < 0. \end{cases}$$

This series in (4.3) has an asymptotic form

$$S_{ASY}(X,Y) = \frac{1}{2ab} \sum_{\substack{m=1 \\ n=0}}^{\infty} \frac{\varepsilon_n}{\sqrt{k_x^2 + k_y^2 - k^2}} \cos(k_x X) \cos(k_y Y) \, . \qquad (4.4)$$

The difference series whose terms consists of the original series terms (4.3) minus the corresponding asymptotic series terms is readily evaluated by digital computer. Thus (4.3) may be evaluated if a method of evaluating the otherwise slowly converging asymptotic series may be found.

To evaluate $S_{ASY}(X,Y)$ (4.4) consider the single series

$$S_o(Y) = \sum_{n=o}^{\infty} \frac{\varepsilon_n}{\sqrt{k_y^2 + u^2}} \cos(k_y Y) \qquad (4.5)$$

where Y is greater than zero and u^2 equals $k_x^2 - k^2$ which is greater than zero under the restriction that ka is less than π. An alternate expression for $S_o(y)$ will be obtained from Poisson's formula [Papoulis 1962]

$$\sum_{n=-\infty}^{\infty} f(nT) = \frac{1}{T} \sum_{n=-\infty}^{\infty} F(\frac{2n\pi}{T}) \tag{4.6a}$$

where f(t) is continuous and its Fourier transform F(ω) is given by

$$F(\omega) = \int_{-\infty}^{\infty} f(t) e^{-i\omega t}\, dt. \tag{4.6b}$$

Equation (4.5) is rewritten as

$$S_o(Y) = y \sum_{n=-\infty}^{\infty} \frac{\cos(n\frac{\pi Y}{b})}{\sqrt{(\frac{n\pi Y}{b})^2 + v^2}} \tag{4.7}$$

where v equals Yu. In (4.6a) f(t) is identified as $\frac{\cos(t)}{\sqrt{t^2 + v^2}}$. Its Fourier transform is given by

$$F(\omega) = \int_{-\infty}^{\infty} \frac{e^{-i\omega t}\cos(t)}{\sqrt{t^2 + v^2}}\, dt \tag{4.8a}$$

$$= \int_{o}^{\infty} \frac{\cos[(1+\omega)t]}{\sqrt{t^2 + v^2}}\, dt + \int_{o}^{\infty} \frac{\cos[(\omega-1)t]}{\sqrt{t^2 + v^2}}\, dt \tag{4.8b}$$

$$= K_o(|1 + \omega|v) + K_o(|\omega - 1|v) \tag{4.8c}$$

Equation (4.8b) follows from (4.8a) plus symmetry considerations. The integrals of (4.8b) result in the modified Bessel functions of (4.8c) [Morse and Feshbach 1953, p. 1323]. Application of (4.6a) to (4.7) yields

$$S_o(Y) = \frac{b}{\pi} \sum_{n=-\infty}^{\infty} [K_o(|Y + 2nb|\sqrt{k_x^2 - k^2}) + K_o(|2nb - Y|\sqrt{k_x^2 - k^2})] \tag{4.9a}$$

$$= \frac{2b}{\pi} K_o(\sqrt{k_x^2 - k^2 Y}) + \frac{2b}{\pi} \sum_{n=1}^{\infty} [K_o([2nb + Y]\sqrt{k_x^2 - k^2})$$

$$+ K_o([2nb - Y]\sqrt{k_x^2 - k^2})]. \tag{4.9b}$$

Applications of (4.9b) to (4.4) yields

$$S_{ASY}(X,Y) = \frac{1}{a\pi} \sum_{m=1}^{\infty} K_o(\sqrt{k_x^2 - k^2}\, Y) \cos(k_x X)$$

$$+ \frac{1}{a\pi} \sum_{m=1}^{\infty} \sum_{n=1}^{\infty} [K_o([2nb + Y]\sqrt{k_x^2 - k^2})$$

$$+ K_o([2nb - Y]\sqrt{k_x^2 - k^2})] \cos(k_x X). \tag{4.10}$$

The second term on the right of (4.10) is very rapidly convergent due to the exponential behavior of K_o's asymptotic expansion [Arfken 1971, p. 517]. The first term on the right (4.10) is exponentially convergent for $Y > 0$. However, as Y becomes smaller the series converges more and more slowly. A summation formula for the first term is given Lewin [1951, p. 83]. Thus

$$\frac{1}{a\pi}\sum_{m=1}^{\infty} K_o\left(\sqrt{k_x^2 - k^2}\, Y\right) \cos(k_x X) = \frac{Y_o(kY)}{4a}$$

$$+ \frac{1}{2\pi} \frac{\cos[k\sqrt{X^2 + Y^2}]}{\sqrt{X^2 + Y^2}} \tag{4.11}$$

$$+ \frac{1}{2\pi}\sum_{n=1}^{\infty} \frac{\cos[k\sqrt{Y^2 + (2na + X)^2}]}{\sqrt{Y^2 + (2na + X)^2}} + \frac{\cos[k\sqrt{Y^2 + (2na - X)^2}]}{\sqrt{Y^2 + (2na - X)^2}}.$$

Note that the dominant singularity in (4.11) is the same as that of the half space dyadic $\overline{\overline{g}}_F$ of Table 1. Unfortunately the infinite series (4.11) is slowly convergent. However if one approximates each term of this series by a finite Taylor series in X and Y about the origin, the summation over n may be obtained by analytical methods. For example, the first term obtained in the Taylor series is given by

$$\sum_{n=1}^{\infty} \frac{\cos(2kan)}{na} = -\ln[2 \sin(ka)] \tag{4.12}$$

[Abramowitz and Stegun 1970, p. 1005]. Similar formulas may be used to evaluate the higher order terms in the Taylor series approximation.

Although the above discussion has been restricted to the evaluation of $g_F^{c,xx}$ only minor changes are needed to evaluate $g_F^{c,yy}$. Also the terms that must be evaluated (3.12) are integrals of the $\hat{x}\hat{x}$ and $\hat{y}\hat{y}$ components of $\overline{\overline{g}}_F^c$. The sums of (4.2) may be evaluated by term integration [Titchmarsh 1939, pp. 36-45]. The exponentially convergent terms (4.10) are also evaluated termwise.

The only remaining question is the accuracy of the previously discussed Taylor series approximation (4.11). A sixth order Taylor series was used for numerical testing and yielded no relative error worse than $1 \cdot 10^{-6}$ in these terms when max(X,Y)/a $\leq$ .05. This procedure allows rapid evaluation of the series on the right of (4.11), provided that both X and Y are small with respect to the cavity dimensions in the aperture plane. Otherwise, this series would not readily yield itself to numerical evaluation on a digital computer.

The above summation techniques are now used to evaluate the $G_A^{c,yy}$ potential terms of (3.12g). Under the thin wire approximation all current is assumed to reside along the wire center. Following Lewin [1975, p. 121] the wire radius is set to zero in all terms except where needed to prevent a divergent series.

To reduce the number of computations necessary to evaluate all of the $G_A^{c,yy}$ terms, this potential is expressed as

$$G_A^{c,yy}(\bar{r}_m|\bar{r}') = S(|y + y'|) + S(|y-y'|) \qquad (4.13)$$

where

$$S(Y) = \frac{1}{2abc} \sum_{\substack{\ell=1 \\ m=1 \\ n=0}}^{\infty} \frac{\varepsilon_\ell \varepsilon_m \varepsilon_n}{K_{\ell mn}^2 - k^2} (ss)_x (ss)_z \cos(k_y Y) \qquad (4.14)$$

and the notation is explained in Table 2. This series may be closed in Y to yield

$$S(Y) = \frac{1}{2abc} \sum_{\substack{\ell=1 \\ m=1}}^{\infty} \frac{\varepsilon_\ell \varepsilon_m (ss)_x (ss)_z \cosh[\sqrt{k_x^2+k_z^2 - k^2}(b-Y)]}{\sqrt{k_x^2 + k_z^2 - k^2} \sinh[\sqrt{k_x^2 + k_z^2 - k^2}\, b]} \cdot \qquad (4.15)$$

This series is rapidly exponentially convergent provided that Y is not too small or does not approach 2b. Since

$$S(Y) = S(2b-Y) \tag{4.16}$$

all that remains to be considered is y small with respect to the cavity dimensions.

A scheme for numerical evaluation of S(Y) with y small is now given. Recall that $\bar{r}_m = (x_c+r_w, y_m, z_c)$ and $\bar{r}' = (x_c, y', z_c)$ where x_c and z_c are the respective x and z coordinates of the wire center. By means of a trig identity S(Y) (4.14) may be expressed as

$$S(Y) = T_2(Y) - T_1(Y) \tag{4.17}$$

where

$$T_1(Y) = \frac{1}{4abc} \sum_{\substack{\ell=1 \\ m=1 \\ n=o}}^{\infty} \varepsilon_\ell \varepsilon_m \varepsilon_n \frac{\cos[k_x(2x_c+r_w)]\cos(k_y Y)(ss)_z}{K_{\ell mn}^2 - k^2} \tag{4.18}$$

and

$$T_2(Y) = \frac{1}{4abc} \sum_{\substack{\ell=1 \\ m=1 \\ n=o}}^{\infty} \frac{\varepsilon_\ell \varepsilon_m \varepsilon_n \cos(k_x r_w) \cos(k_y Y)}{K_{\ell mn}^2 - k^2} (ss)_z \quad . \tag{4.19}$$

Equation (4.18) may be closed in x to yield a rapid exponentially converging series. The wire radius in (4.18) is set to zero. Next (4.19) is closed in z to yield

$$T_2(y) = \frac{1}{4abc} \sum_{\substack{m=1 \\ n=o}}^{\infty} \frac{\varepsilon_m \varepsilon_n}{\sqrt{k_x^2 + k_y^2 - k^2}} \frac{\cos(k_y Y) \sinh[\sqrt{k_x^2+k_y^2-k^2}\,(C-Z)}{\sinh[\sqrt{k_x^2 + k_y^2 - k^2}\, C]} \quad (4.20)$$

This series has the asymptotic from $S_{ASY}/2$. (4.4). Thus the procedure for evaluation of this term has already been given.

CHAPTER 5

SAMPLE NUMERICAL RESULTS

The numerical solution scheme of the previous sections was implemented by means of a fortran program on a Cyber 175 computer. In all examples (Figures 7,10,14) the wire radius was set at one millimeter, the number of aperture pulses in the x-direction was 4, the number of aperture pulses in the y-direction was 5, and the number of wire current pulses was 12; a zero half pulse counts as one half.

In the first example (Figure 7) a normally incident plane wave, with free-space wavelength equal to 10 meters, impinges on a cavity backed aperture. The incident electric field is y directed to give maximum coupling to the interior wire. The cavity dimensions are a = 1.4 meters, b = 4.5 meters, and c = 2.4 meters in the x, y, and z dimensions respectively. The square .02m x .02m aperture is centered with midpoint $\bar{r}_a$ = (.7,2.25,1.2). The centered thin wire runs from (.7,.5,1.2) to (.7, 4.,1.2). Figures 8 and 9 show some cuts of the aperture electric field. As expected for electrically small apertures the aperture electric field is essentially imaginary. The real part is seven orders of magnitude lower than the imaginary part. The y component of the aperture electric field has even symmetry about both axes of the aperture, while the x component is odd. Figures 10 and 11 show a comparison between Seidel's

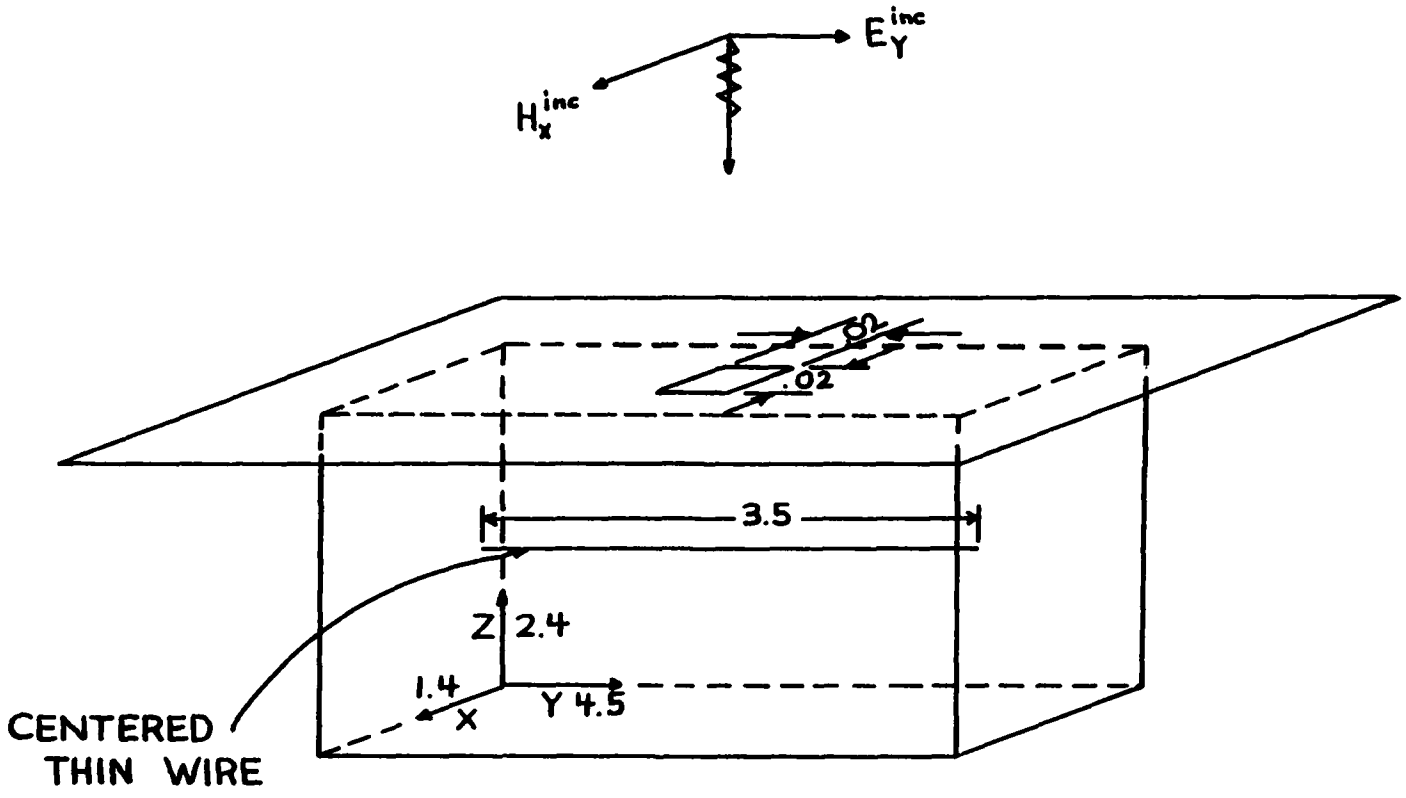

Figure 7 Problem Geometry 1.

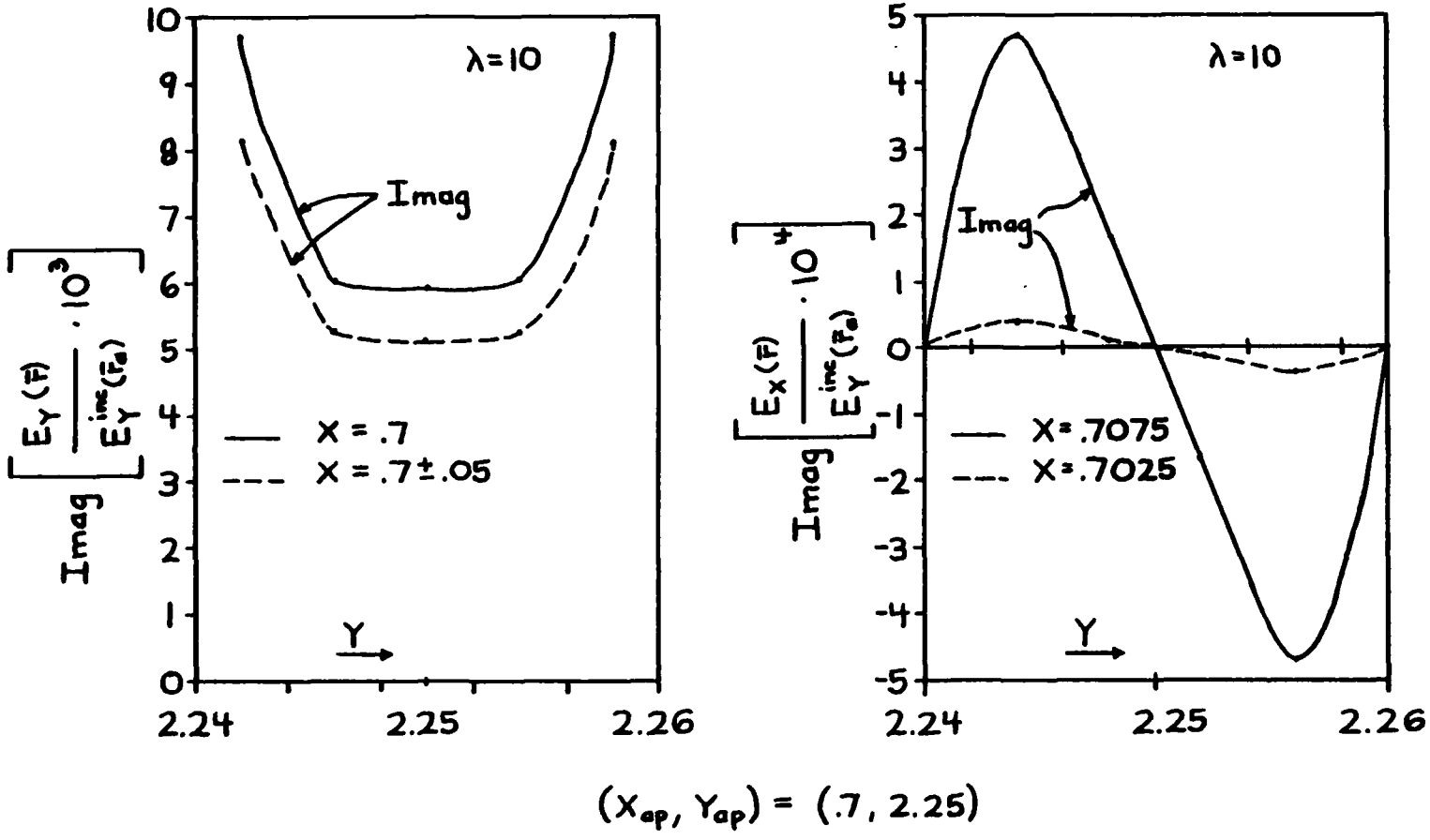

Figure 8 Aperture Electric Fields for Problem Geometry 1.

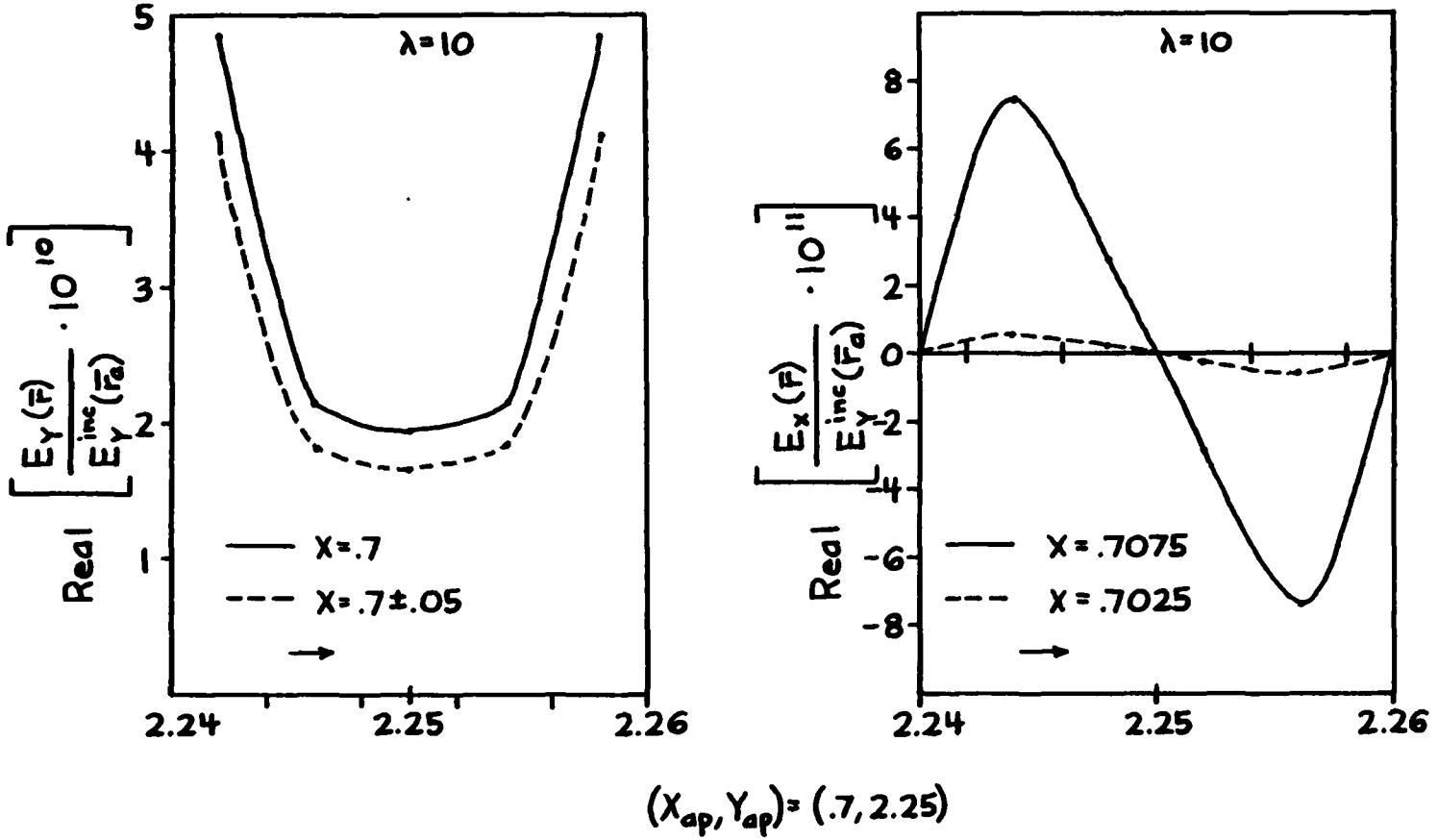

Figure 9. Real Aperture Electric Fields For Problem Geometry 1.

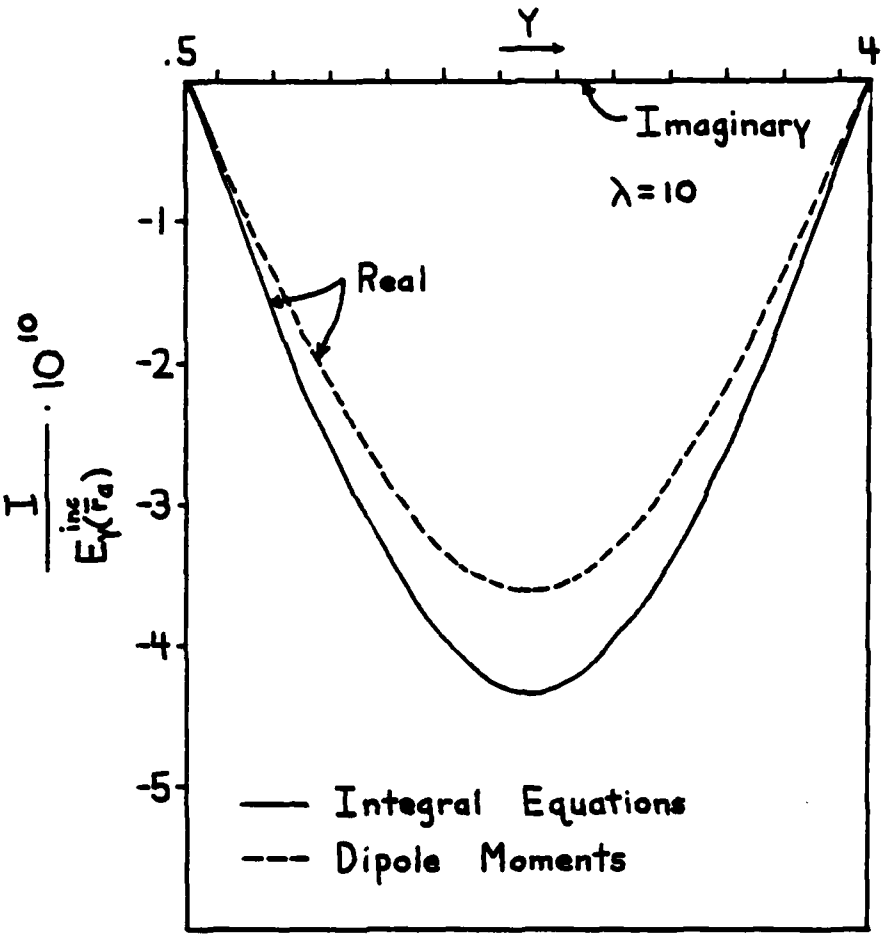

Figure 10 Wire Currents for Problem Geometry 1.

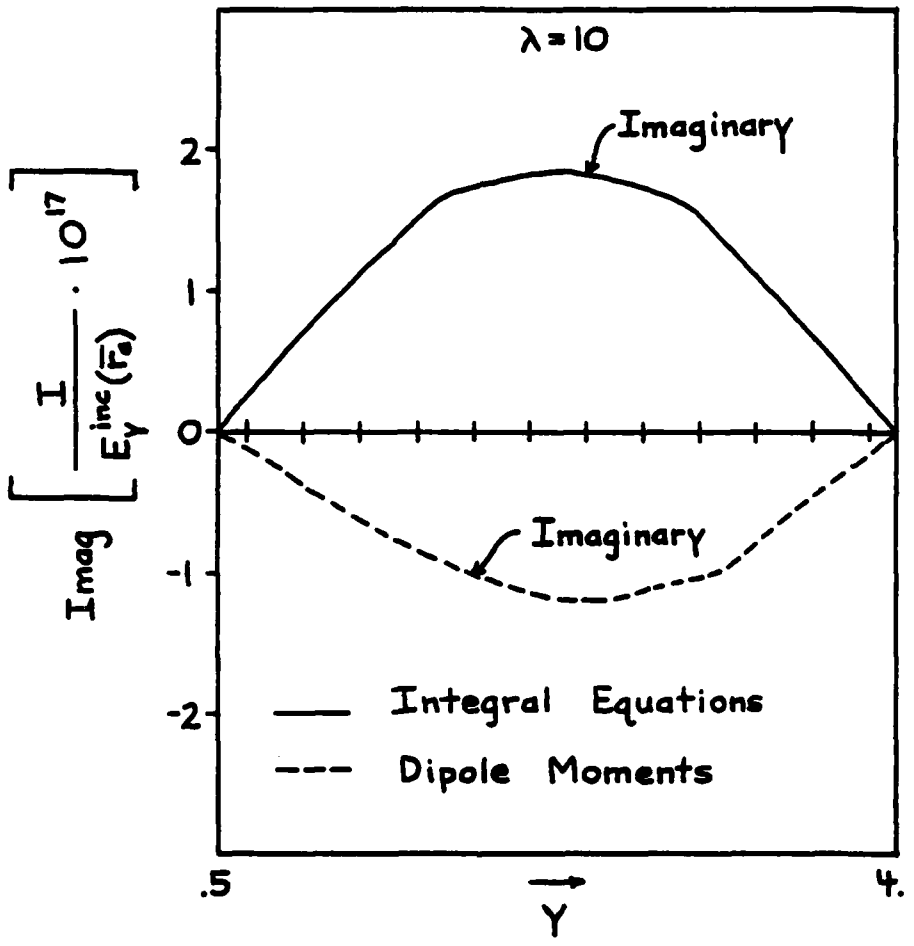

Figure 11 Imaginary Wire Currents for Problems Geometry 1.

dipole moment solution [Seidel 1977, 1978] (dotted line) and the integral equation approach (solid line). Seidel's solution treated the aperture coupling by the use of dipole moments for elliptical apertures, in this case circular with radius .01 m and located inside the square aperture. Unfortunately a sign discrepancy occurs in the imaginary part of the current (Figure 11). Note that while the symmetry of the integral equation method is preserved the dipole moment has lost its symmetry. At first one might suspect that the imaginary part of the current (Figure 11) is in the noise, however after running various test cases this sign discrepancy consistently occurred. A painstaking search of our computer program yielded no error. An attempt to resolve this discrepancy is given in Appendix A.

In the next example (Figure 12) an incident plane wave travels in the $\hat{y}$ direction, is polarized with a $\hat{z}$ directed incident field, and has free-space wavelength equal to one meter(1m). The cavity dimensions are .25m, .3m, and .2m in the x, y, and z directions respectively. The wire is oriented parallel to the y axis and runs from (.125,.05,.1) to (.125, .25,.1). The square aperture (.02m x .02m) is centered with midpoint $\bar{r}_a$ = (.125,.15,.2). Figures 13 and 14 show cuts of the aperture electric fields. the symmetry of the aperture electric fields is described in Table 3. Figure 15 gives a comparison between the wire currents computed by Seidel's

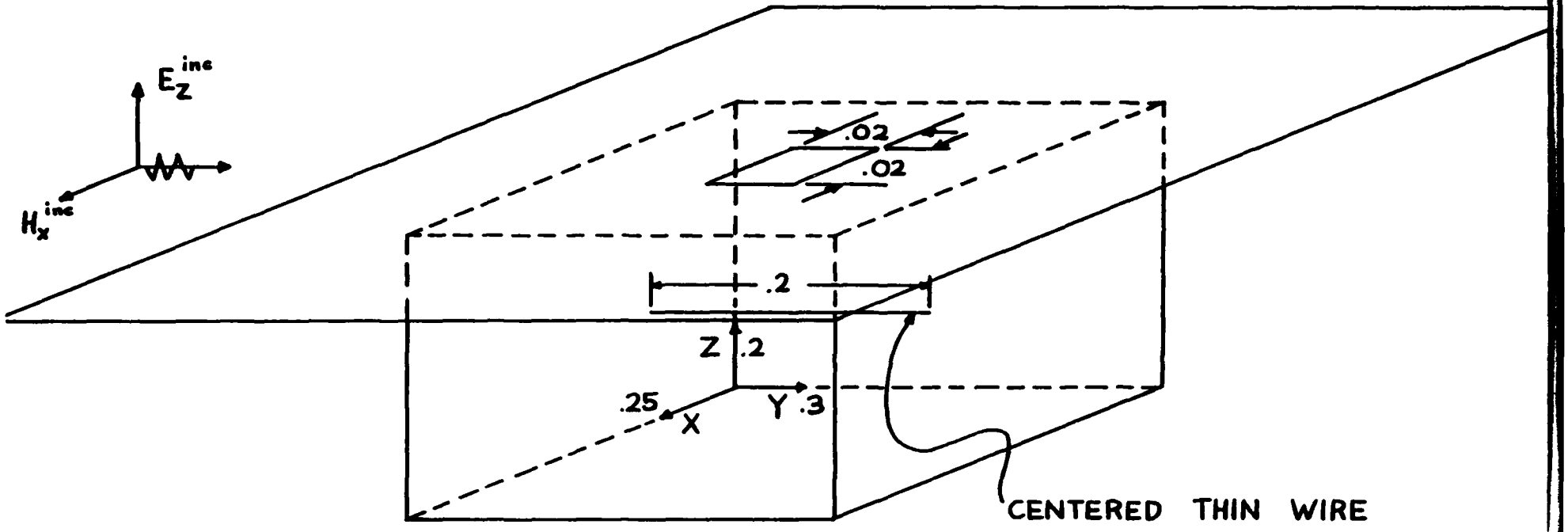

Figure 12 Problem Geometry 2

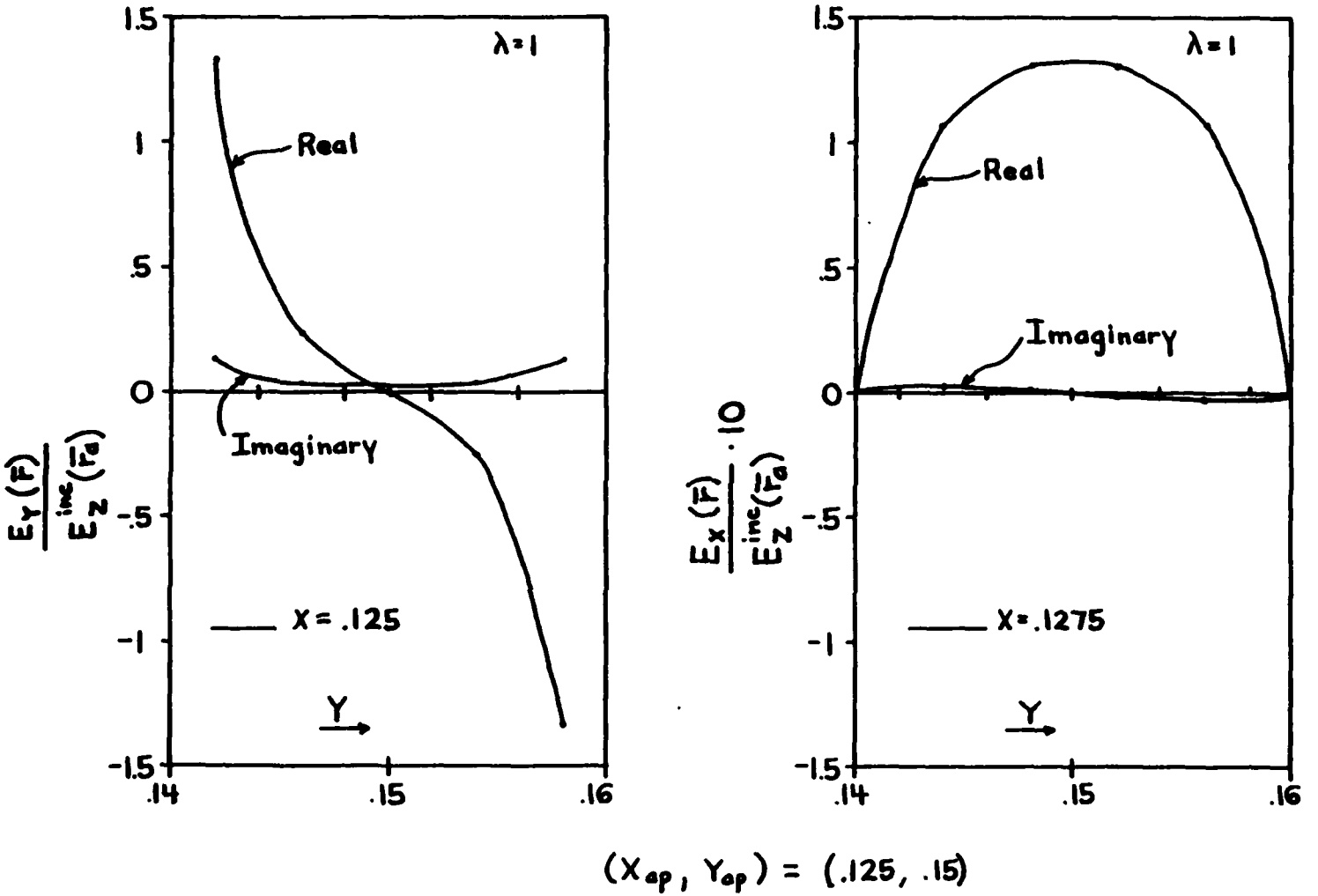

Figure 13. Aperture Electric Fields for Problem Geometry 2.

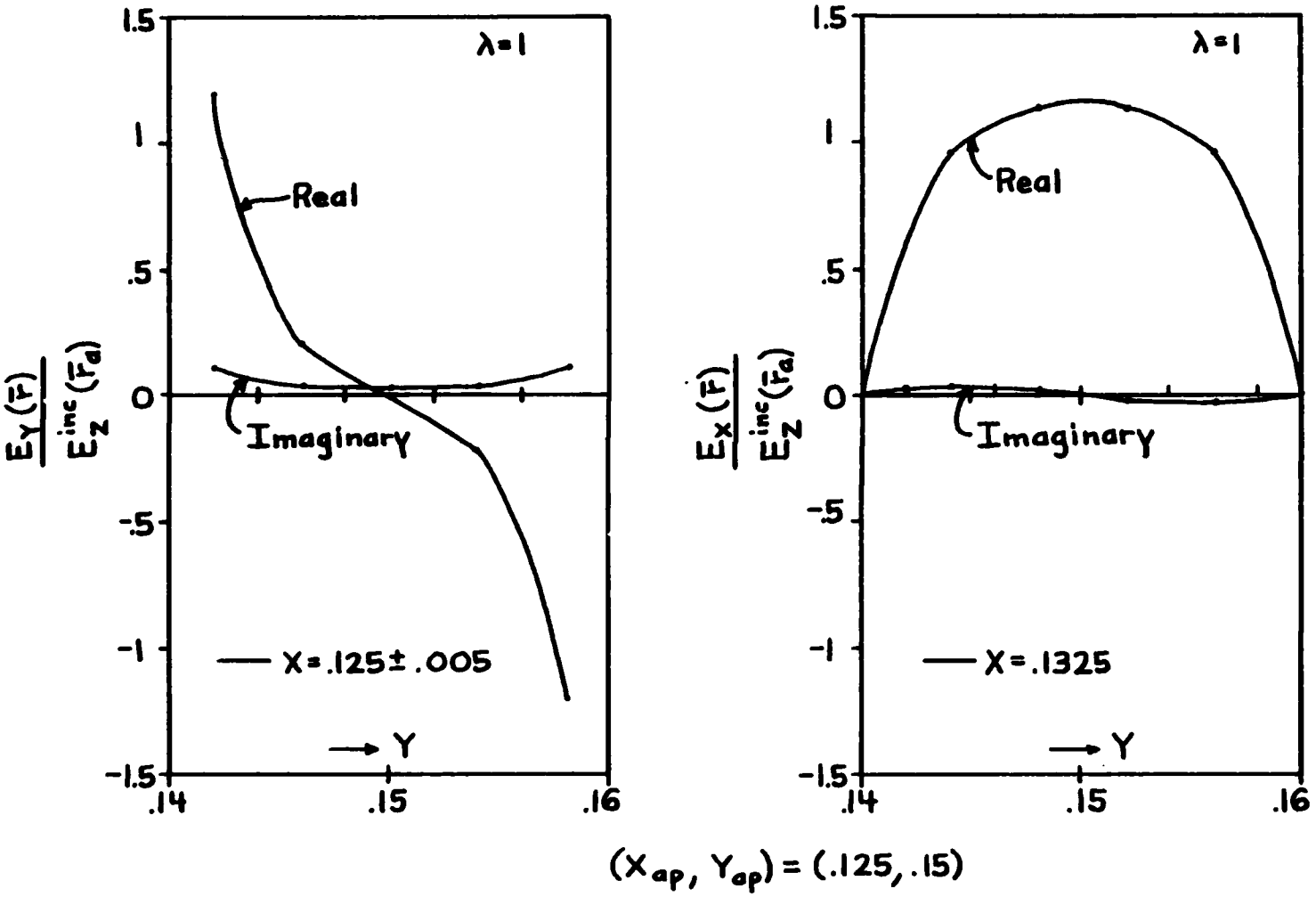

$(X_{ap}, Y_{ap}) = (.125, .15)$

Figure 14. Aperture Electric Fields for Problem Geometry 2.

Table 3 Aperture Electric Field's Symmetry for Geometry 2.

Component	Real or Imaginary	Aperture x-axis	Aperture y-axis
x	real	odd	even
x	imaginary	odd	odd
y	real	even	odd
y	imaginary	even	even

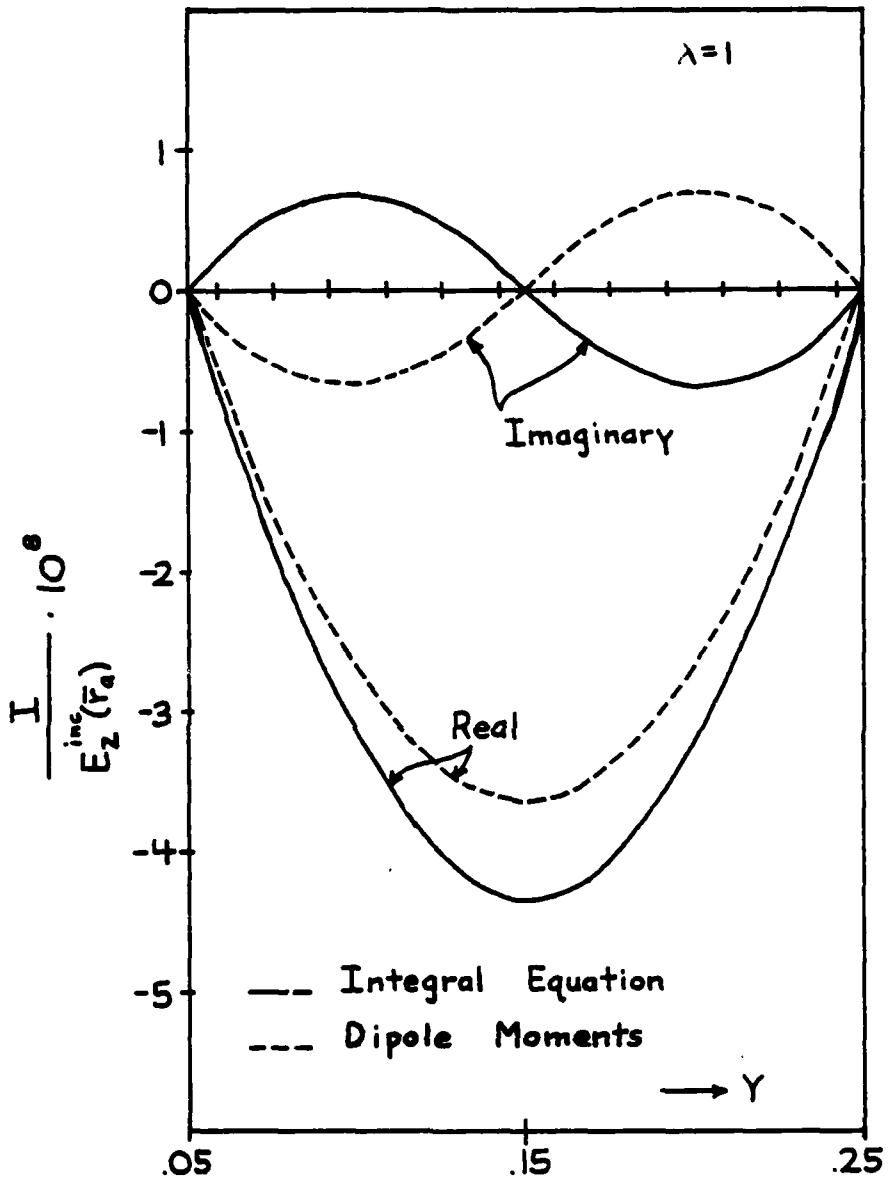

Figure 15. Wire Currents for Problem Geometry 2.

dipole moment approach and the technique presented in this paper. The dipole moment solution is for a circular aperture of radius .01m and with centerpoint $\bar{r}_a$ = (.125,.15,.2). Again the sign discrepancy persists.

Figure 16 has the same geometry as Figure 7 except the centered aperture is made rectangular (.8m x .3m). A study of wire current versus frequency is made in Figures 17 - 21. Figures 7, 8, 9, and 20 show the variation in current for frequencies of 10^4. 4.10^4 · 10^8 hertzs respectively. Note the change in sign of the wire current as the frequency crosses the first wire resonance of $4.16 \cdot 10^7$ hertzs. This resonant frequency is slightly lower than that for a wire in free space. Figures 21 and 22 show the variation of the current at the wire center with frequency. Note that the real part of the current (Figure 21) is proportional to the frequency squared in the quasi-static portion of the frequency spectrum. Also the imaginary part of the current (Figure 22) is proportional to the fifth power of the frequency in the quasi-static region. The amount of computation time for each frequency point is 20 seconds c.p.u. time on the Cyber 175 computer.

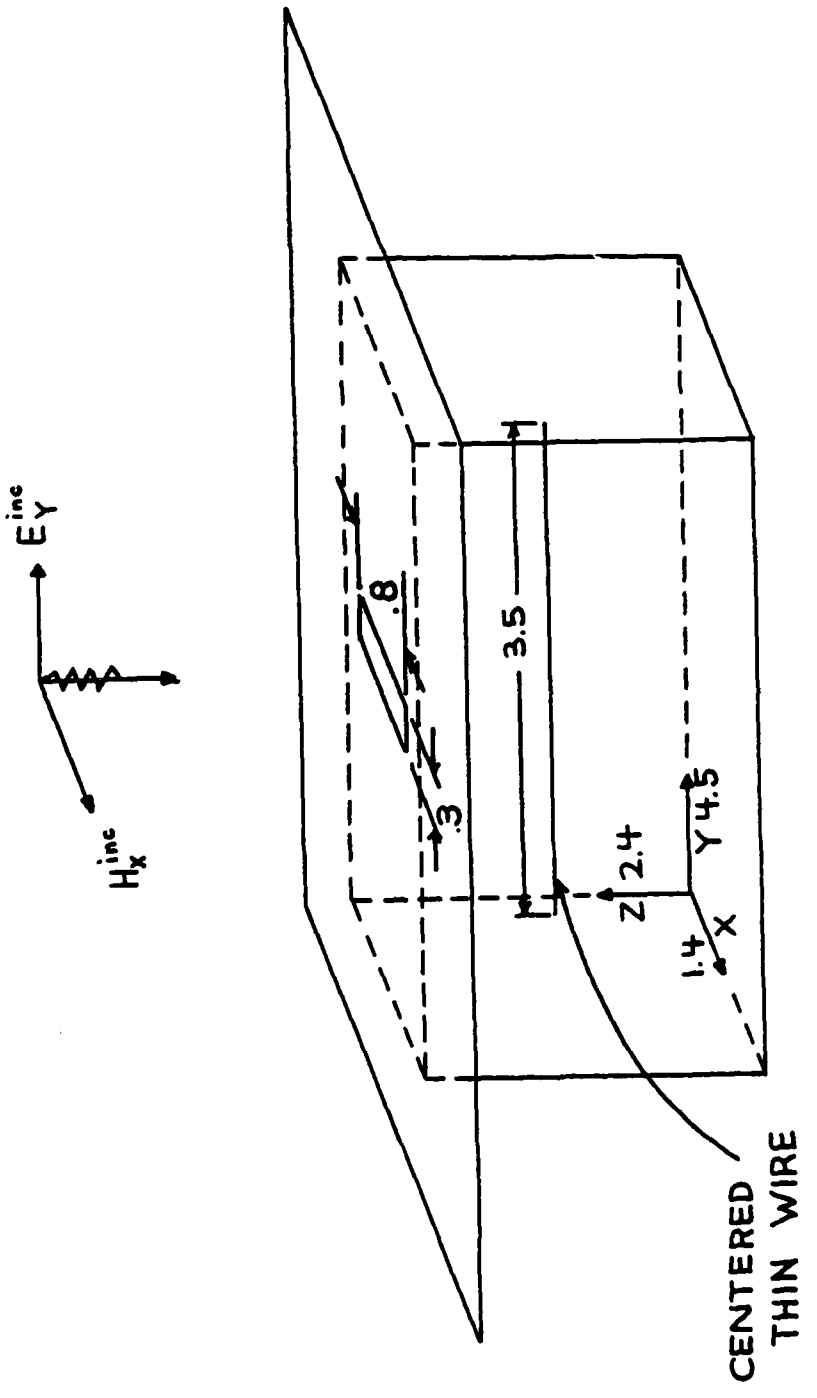

Figure 16. Problem Geometry 3.

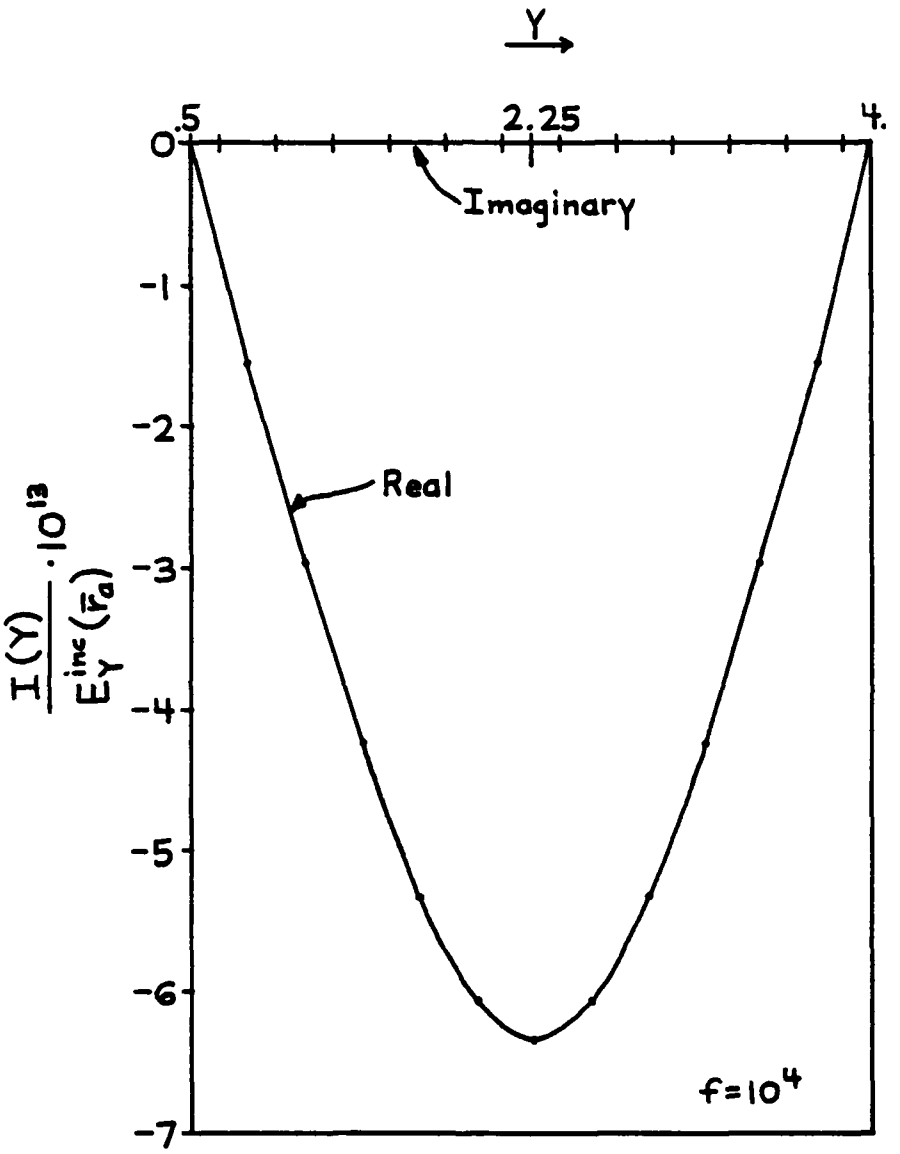

Figure 17. Wire Currents for Geometry 3.

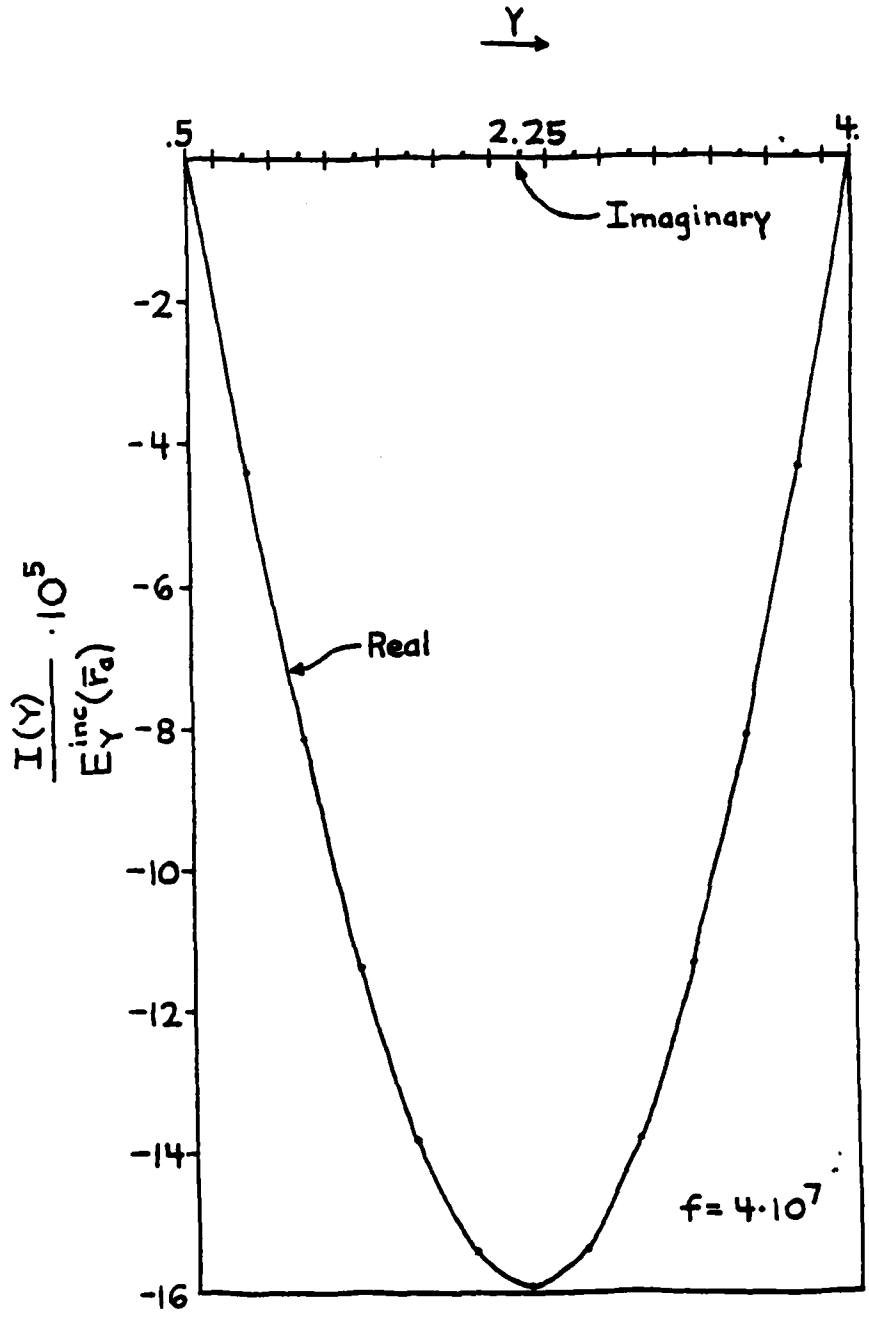

Figure 18. Wire Currents for Geometry 3.

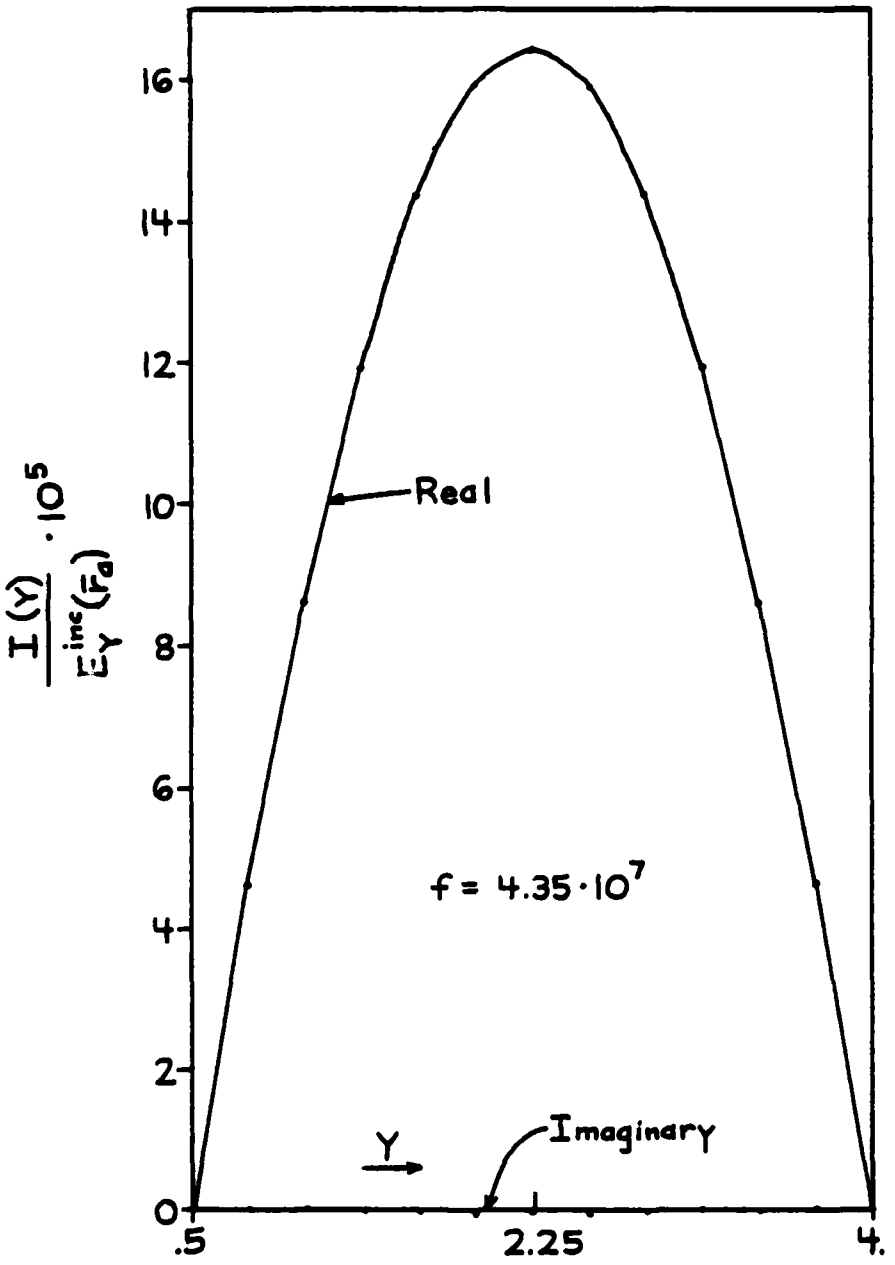

Figure 19. Wire Currents for Geometry 3.

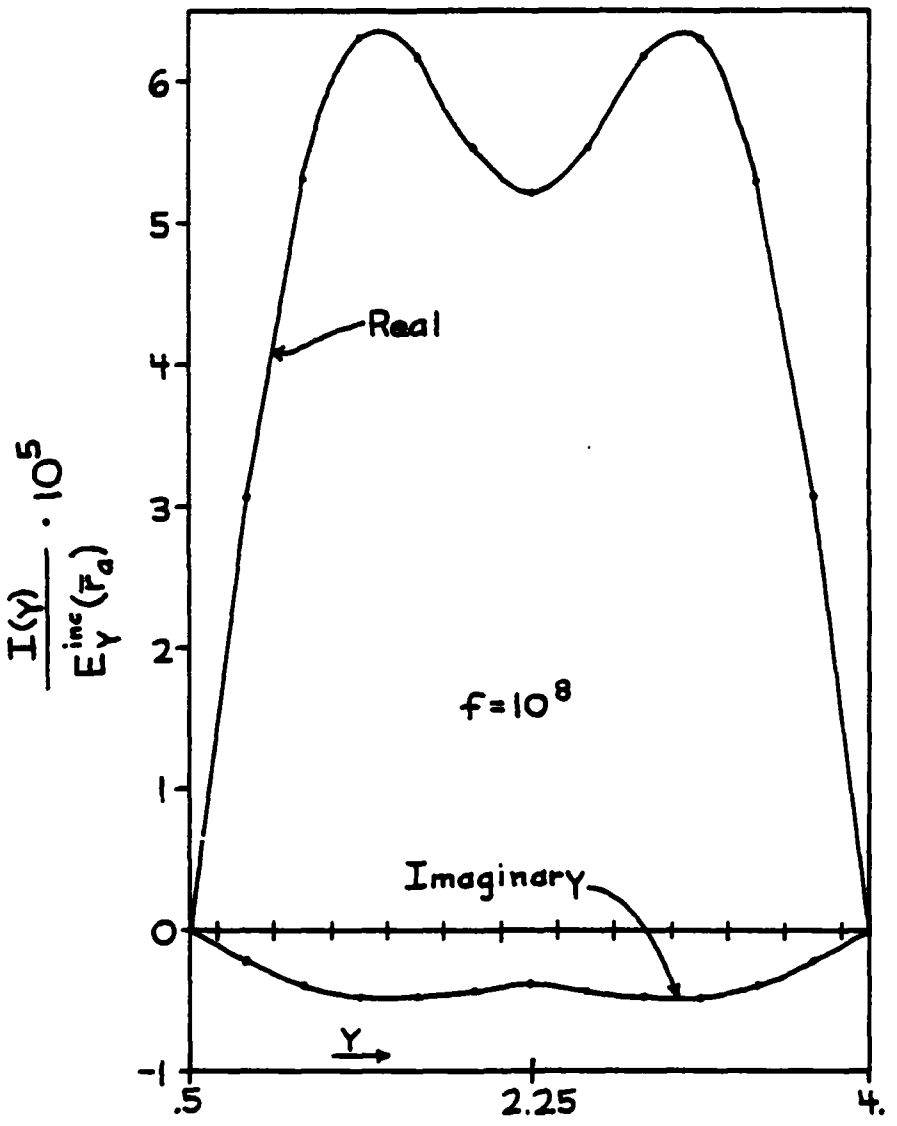

Figure 20. Wire Currents for Geometry 3.

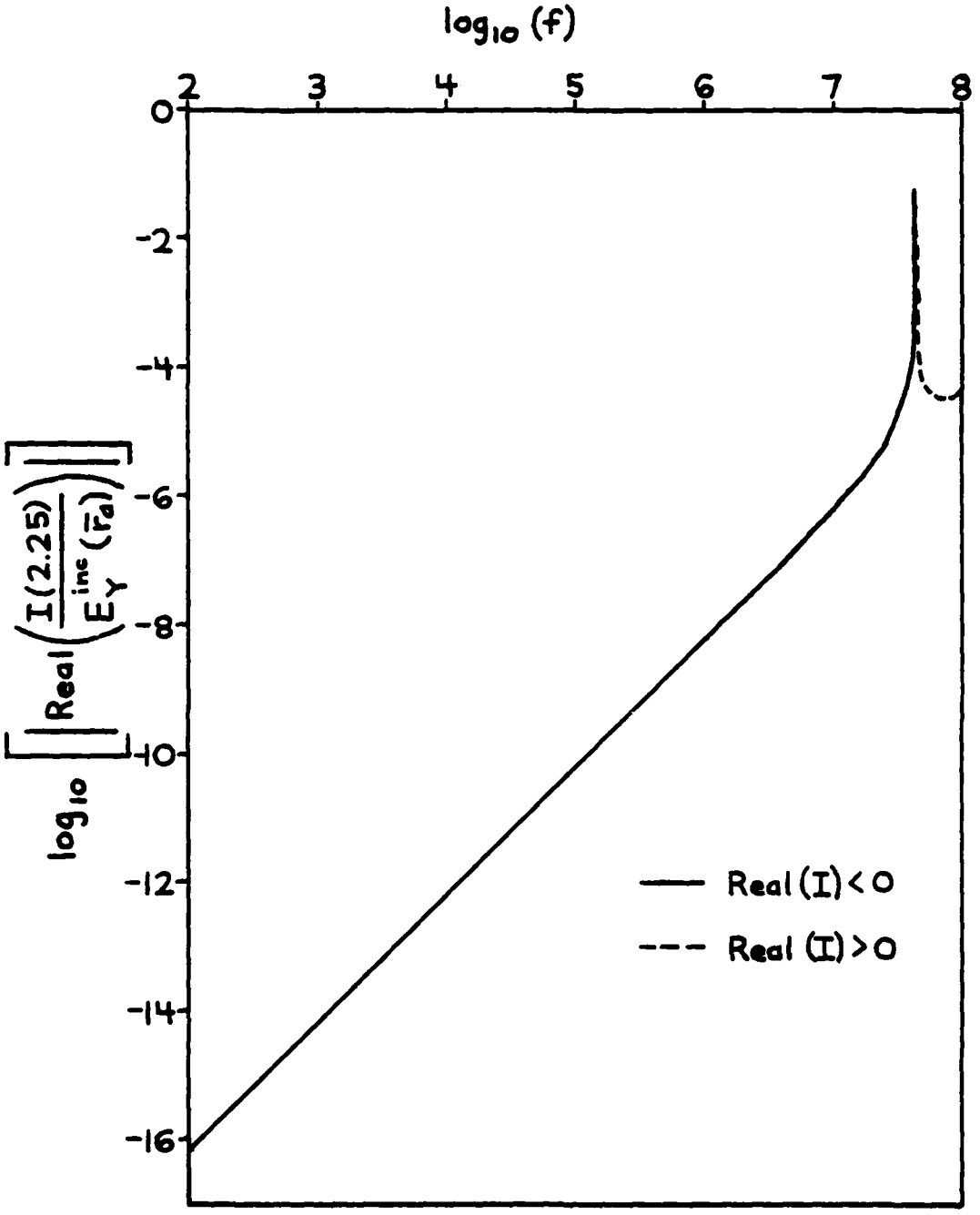

Figure 21. Real Current at Wire Center vs. Frequency (Geometry 3).

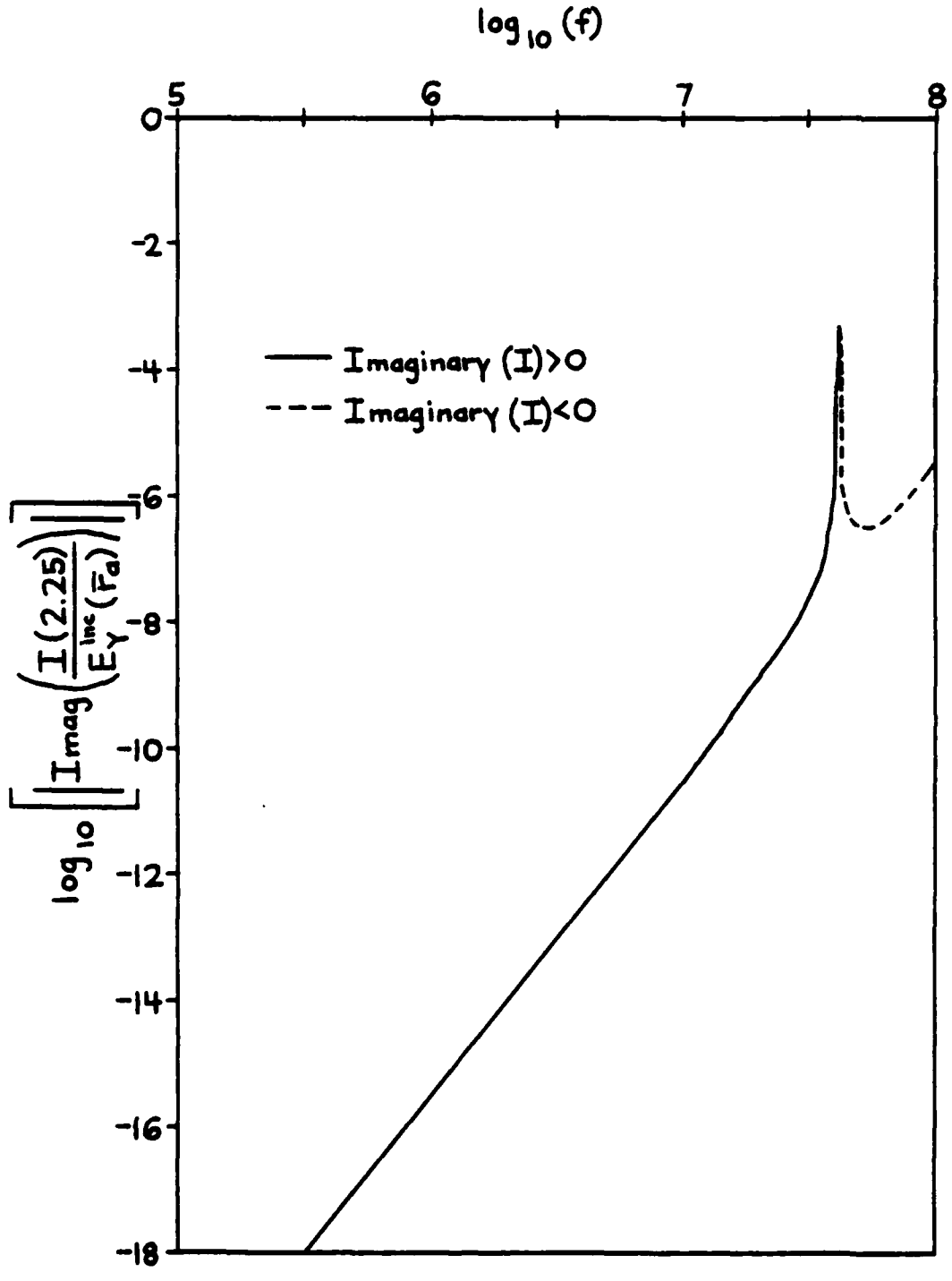

Figure 22. Imaginary Current at Wire Center vs. Frequency (Geometry 3).

APPENDIX A

ON THE SIGN DISCREPANCY

In this appendix analytical techniques are combined with numerical results in an attempt to resolve the sign discrepancy of Chapter 5. In particular the problem geometry of Figure 7 will be considered. First check on the signs of the aperture electric fields will be made by comparison with currents induced when a normally incident plane wave strikes a thin perfectly conducting rectangular plate. If one neglects the contributions to the aperture fields due to scattering from the wire and cavity walls these problems are Babinet equivalents.

The currents induced on the plate (Figure 23) satisfy

$$-i\omega\varepsilon\, E_y^{inc}(\bar{r}) = (k^2+\frac{\partial^2}{\partial x^2})\iint_P \frac{J_x(\bar{r})e^{-ikR}}{4\pi R}dx'dy' + \frac{\partial^2}{\partial x\partial y}\iint_P \frac{J_y(\bar{r})e^{-ikR}}{4\pi R}dx'dy' \tag{A.1}$$

$$-i\omega\varepsilon\, E_y^{inc}(\bar{r}) = (k^2+\frac{\partial^2}{\partial x^2})\iint_P \frac{J_y(\bar{r}')e^{-ikR}}{4\pi R}dx'dy' + \frac{\partial^2}{\partial x\partial y}\iint_P \frac{J_x(\bar{r}')e^{-ikR}}{4\pi R}dx'dy' \tag{A.2}$$

where $\bar{r}$ is located on the plate surface P, and $R = |\bar{r}-\bar{r}'|$. For a normally incident H_y polarized plane wave (Figure 23) (A.1) and (A.2) may be expressed as

$$\frac{-\partial H_y^{inc}(\bar{r})}{\partial z} = (k^2+\frac{\partial^2}{\partial x^2})\iint_P \frac{J_x(\bar{r}')e^{-ikR}}{4\pi R}dx'dy' + \frac{\partial^2}{\partial x\partial y}\iint_P \frac{H_x(\bar{r})e^{-ikR}}{4\pi R}dx'dy' \tag{A.3}$$

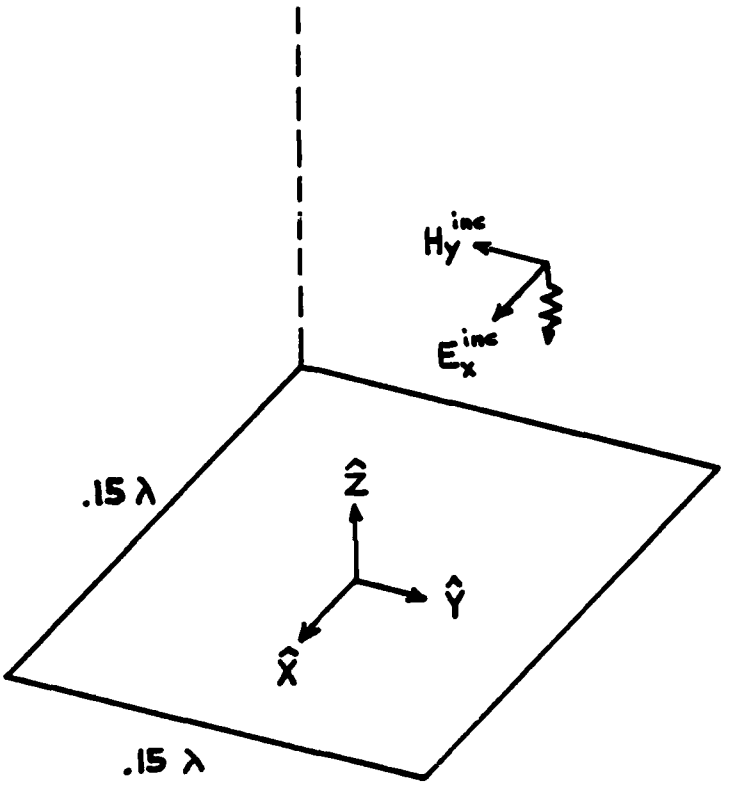

Figure 23 Scattering from a square plate.

$$0 = (k^2 + \frac{\partial^2}{\partial y^2}) \iint_P \frac{H_y(\bar{r}')}{4\pi R} e^{-ikR} dx'dy' - \frac{\partial^2}{\partial x \partial y} \iint_P \frac{H_y(\bar{r})}{4\pi R} e^{-ikR} dx'dy' \qquad (A.4)$$

If one neglects the contribution of the aperture fileds due to the wire and side and back cavity walls and specializes the incident field to an E_y polarized normally incident field (2.7a) and (2.7b) become

$$0 = (k^2 + \frac{\partial^2}{\partial y^2}) \iint_A \frac{E_x(\bar{r}')}{2\pi R} e^{-ikR} dx'dy' \; \frac{\partial^2}{\partial y \partial x} \iint_A \frac{E_y(\bar{r}')e^{-ikR}}{2\pi R} dx'dy' \qquad (A.5)$$

$$-\frac{\partial E_y^{inc}(\bar{r})}{\partial z} = (k^2 + \frac{\partial^2}{\partial x^2}) \iint_A \frac{E_y(\bar{r}')e^{-ikR}}{2\pi R} dx'dy' - \frac{\partial^2}{\partial x \partial y} \iint_A \frac{E_x(\bar{r}')e^{-ikR}}{2\pi R} dx'dy'. \qquad (A.6)$$

If one identifies $E_y^C = \frac{1}{2}H_y^P = -\frac{J_x^P}{2}$ and $E_x^C = \frac{H_x^P}{2} = J_y^P$ where the superscripts "C" and "P" denote cavity and plate respectively, one sees that for identical forcing functions $H_y^{inc} = 1$ and $E_y^{inc} = 1$, the aperture E_y^C should be $-\frac{1}{2} J_x^P$.

Figure 24 shows a plate scattering problem for a .15λ square plate with $H_y^{inc} = -1$. When comparing with Figures (8 and 9) with $E_y^{inc} = 1$ we should have E_y^C to have the same sign as J_x^P, as is indeed the case. Note that the signs of the aperture fields and wire currents should not change in the quasi-static frequency regime. The sign discrepany of Chapter 5 is in the imaginary part of the wire current. Since the Greens functions of (2.7c) are real the imaginary component of the wire current is driven by the real part of the aperture

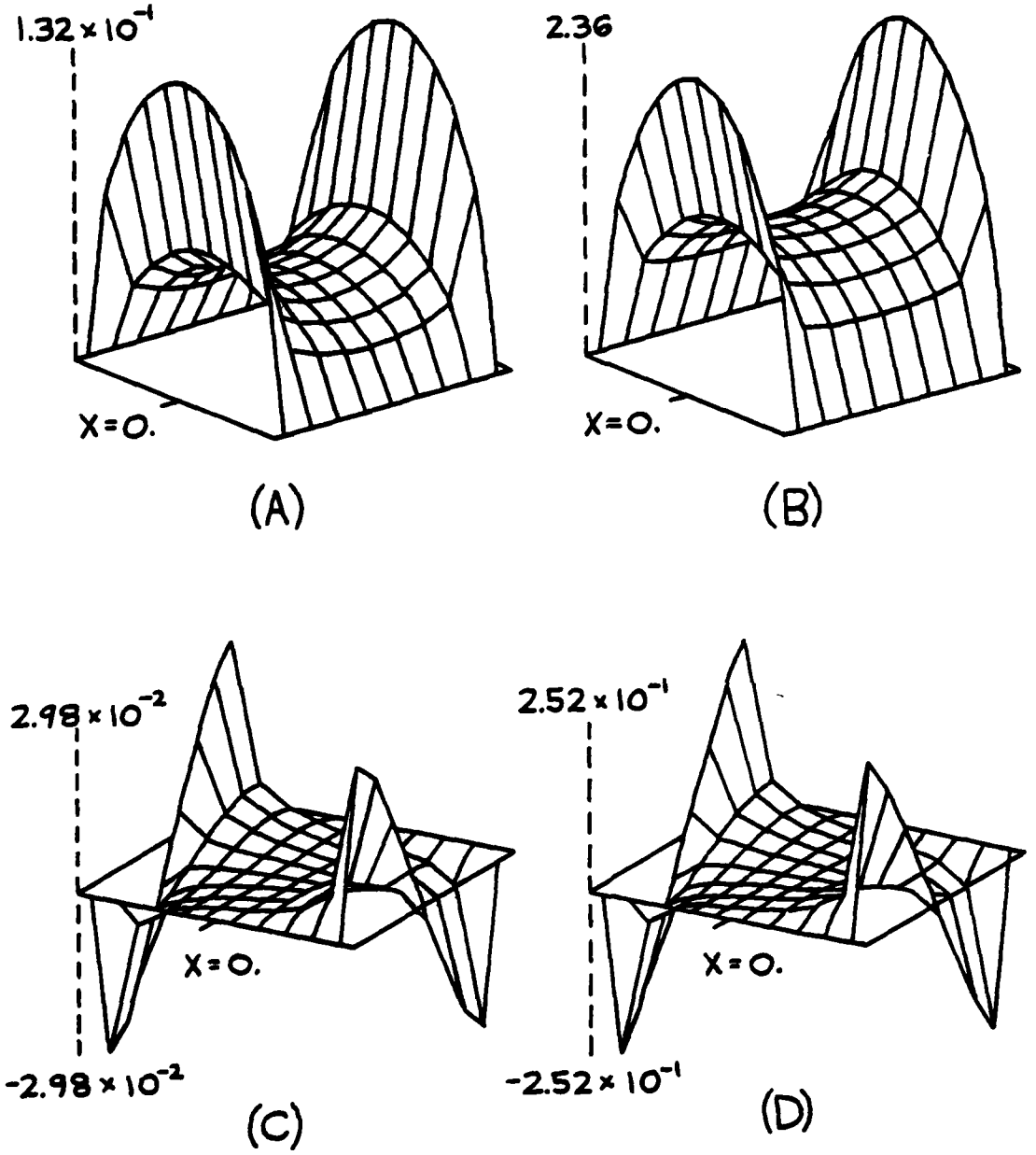

Figure 24 Current induced on a (.15λ x .15λ) square plate for a normally incident excitation with $H_y^{INC} = -1$ on the plate. (a) $R_e(J_x)$, (b) $I_m(J_x)$, (c) $R_e(J_y)$, (d) $I_m(J_y)$.

field E_y. The question arises as to whether the presence of the cavity and or wire changes the sign of the real part of the aperture field E_y. The results of our computations indicate that this is not the case, as illustrated in Figures (25-28).

The imaginary component decreases by approximately factor of 2 as the Green's functions kernel in (A.5) and (A.6) changes from

$$\frac{1}{2\pi}\left(\frac{\cos(kR)}{R} - i\,\frac{\sin(kR)}{R}\right) \qquad (A.7)$$

for the halfpace to approximately

$$\frac{1}{2\pi}\left(\frac{\cos kR}{R} - i\,\frac{\sin(kR)}{2R}\right. \qquad (A.7)$$

for the interior cavity, exterior halfspace problem. It is comforting to note that decreasing the imaginary part of the kernel also reduced the real part of E_y', since an entirely real kernel in (A.5) and (A.6) would produce a zero real component of both E_y and E_x.

An argument is now given to determine the sign of the imaginary wire current (Figure 11). Note that (2.7C) may be expressed as

$$J_y(\bar{r}) = i\omega\varepsilon\,\Theta(E_y) \qquad (A.7)$$

where Θ is a real linear operator. Note that the real and imaginary parts of E_y have approximately the same shape. Also note that the imaginary part of E_y, E_y^i produces an negative real current (Figure 10). Thus $\Theta(E_y^i)$ is positive. Since the

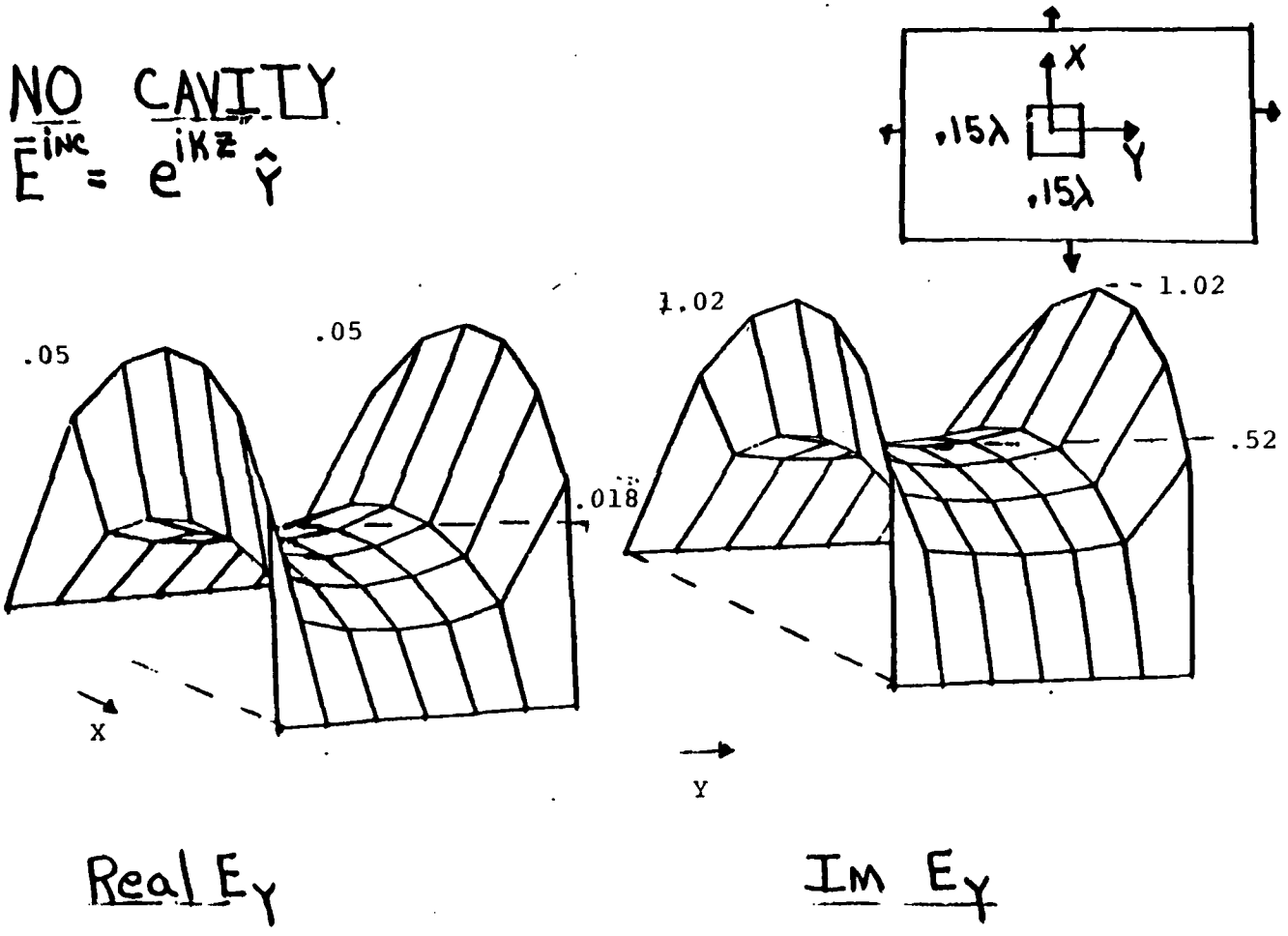

Figure 25 Aperture Electric Fields

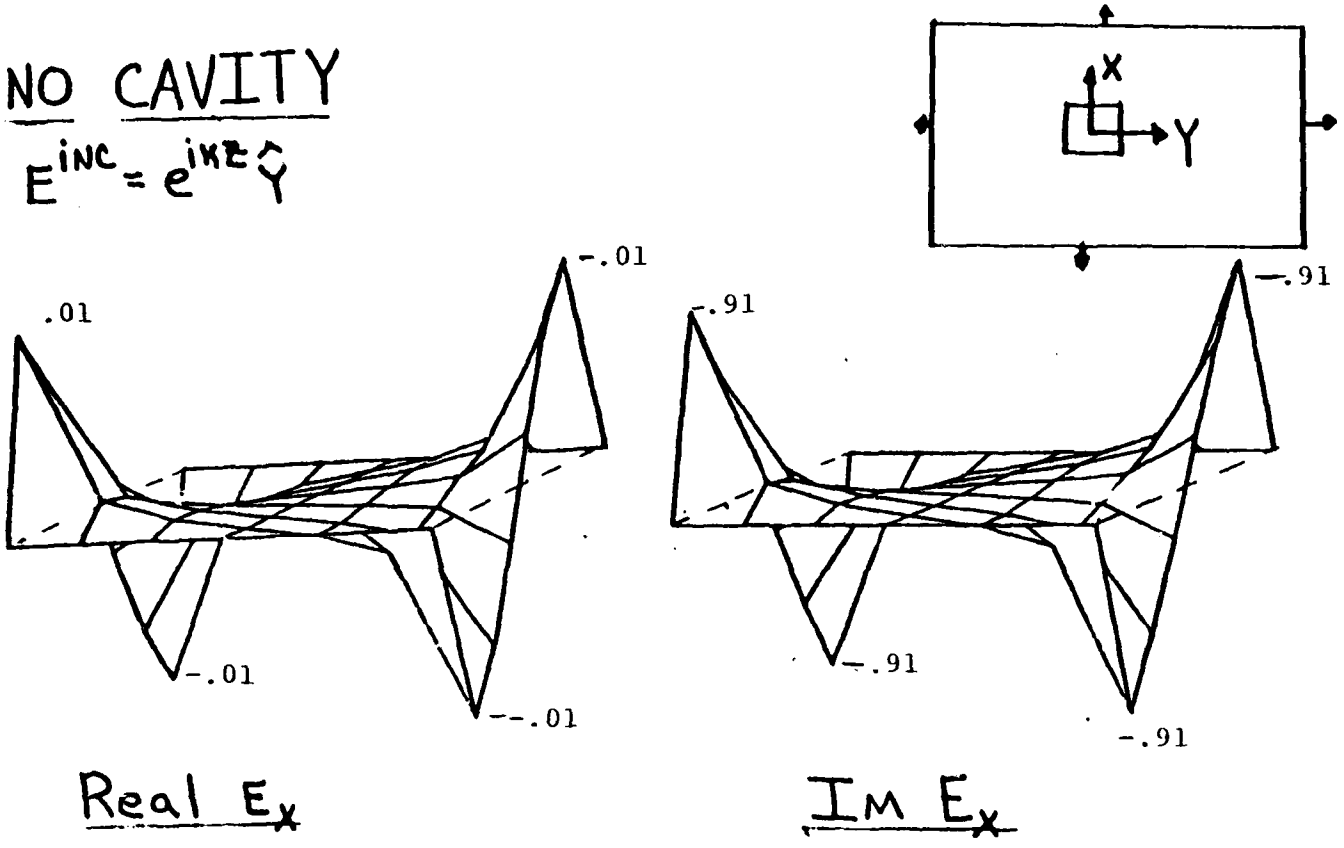

Figure 26 Aperture Electric Fields

APERTURE ELECTRIC FIELDS

$$\bar{E}^{inc} = e^{jk(z-\gamma_3)}\,\hat{y}$$

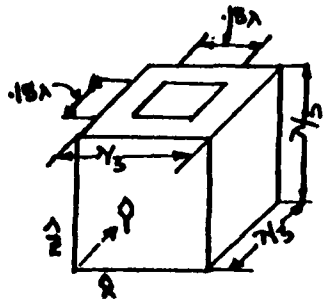

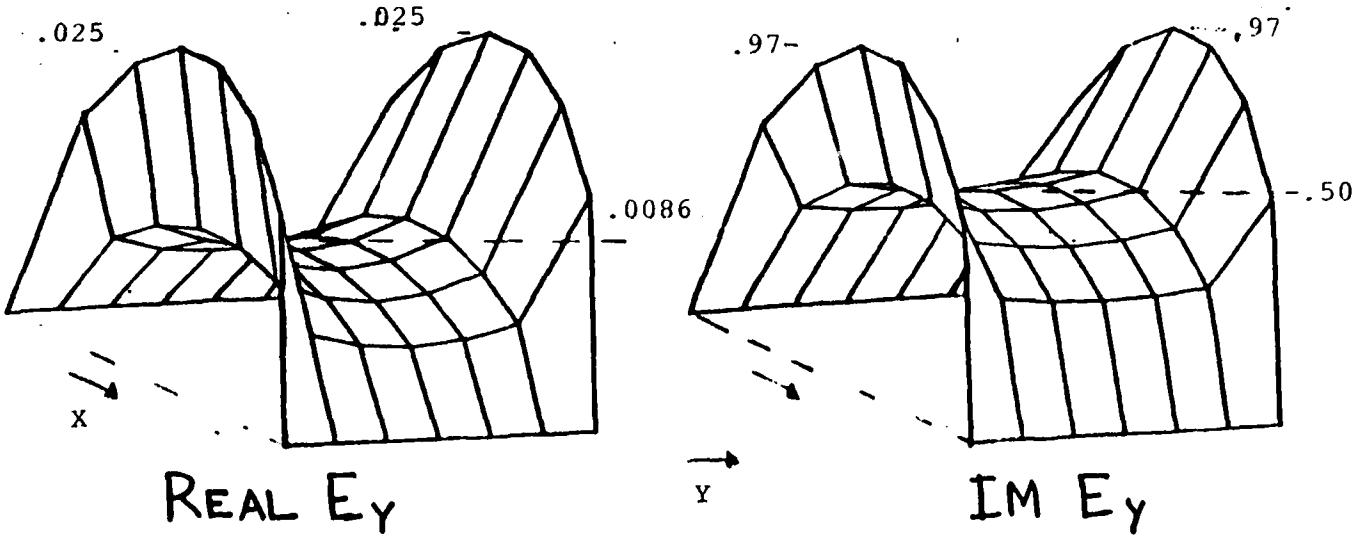

Figure 27 Aperture Electric Fields

APERTURE ELECTRIC FIELDS

$$\bar{E}^{INC} = e^{jk(z-\lambda/3)}\hat{\phi}$$

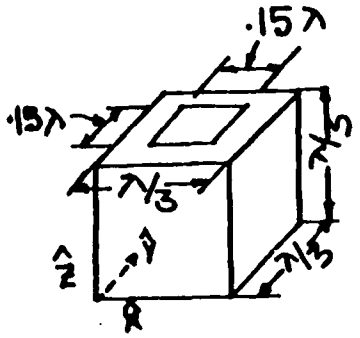

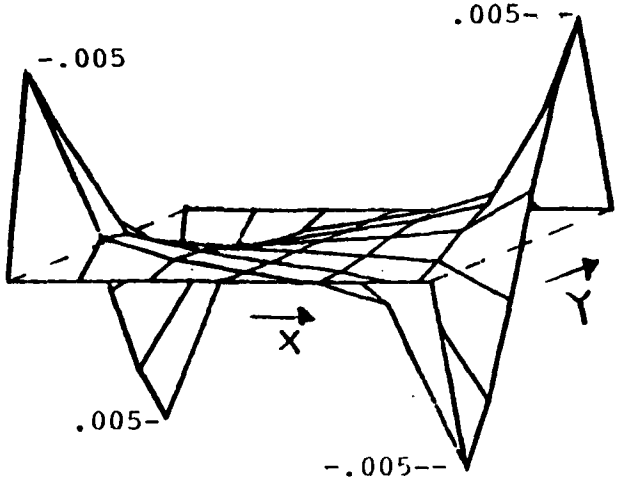

REAL E_x

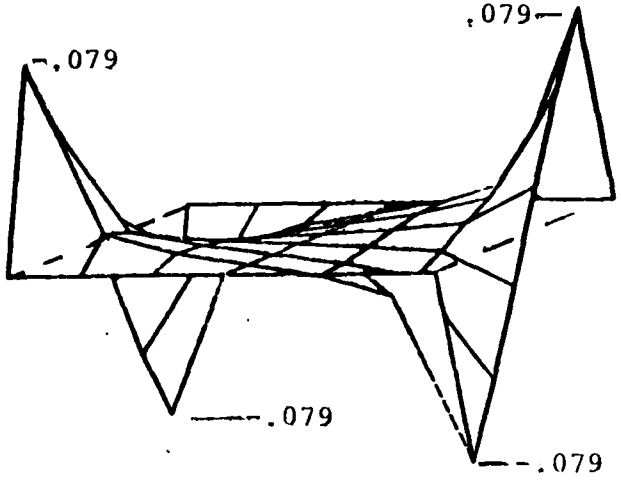

IM E_x

Figure 28 Aperture Electric Fields

real part of $E_y(E_y^r)$ has approximately the same shape it follows that $\theta(E_y^r)$ is again positive, so that the imaginary part of J_y (Figure 11) should be positive.

REFERENCES

Abramowitz, N. and I. Stegun. Handbook of Mathematical Functions, New York: Dover, 1970.

Arfken, G. Mathematical Methods for Physicists, Second Ed., New York: Academic Press, 1971.

Gradshteyn, I. S. and I. M. Ryzhik. Tables of Integrals Series and Products, Fourth Ed., New York: Academic Press, 1965.

Harrimgton, R. F. Time-Harmonic Electromagnetic Fields, New York; McGraw-Hill, 1961.

_____. Field Computation by Moment Methods, New York; MacMillan, 1968.

Johnson, W. A., A. Q. Howard, and D. G. Dudley, "On the Irrational Component of The Electric Green's Dyadic", Radio Science, Vol. 14, No. 6, pp. 961-967, Nov-Dec., 1979.

Levin, L. Theory of Waveguides, London: Newmes-Butterworths, 1975.

_____. Advanced Theory of Waveguides, London" Iliffe and Sons, 1951.

Meixner, J. "The Behavior of Electromagnetic Fields at Edges," IEEE Trans. Antennas Propagat., Vol. AP-21, pp. 442-446, July 1972.

Morse, R. M. and H. Feshbach. Methods of Theoretical Physics, Parts I and II, New York: McGraw-Hill, 1953.

Papoulis, A. The Fourier Integral and Its Applications, New York; McGraw-Hill, 1962.

Seidel, D. B. "Aperture Excitation of a Wire in a Cavity, Part I," Air Force Office of Scientific Research, Report 1876-2, June 1977.

_____. "Aperture Excitation of a Wire in a Cavity," IEEE Trans. MTT. Vol. 26, pp. 908-914, Nov. 1978.

Spiegel, M. R. Complex Variables, New York; McGraw-Hill, 1964.

Titchmarsh, E. C. The Theory of Functions, Second Ed., London: Oxford, University Press, 1939.

Wilton, D. and A. W. Glisson "Toward Simple Efficient Numerical Techniques for Scattering by Surfaces," A.P.S. Int. Symp. Digest, pp. 515-518, Amherst, Mass., Oct. 1976.